Cooperative actin filament nucleation by the Arp2/3 complex and formins maintains the homeostatic cortical array in Arabidopsis epidermal cells

Liyuan Xu[1], Lingyan Cao[1], Jiejie Li[1], Christopher J. Staiger[1,2,3,*]

[1] Department of Biological Sciences, Purdue University, West Lafayette, IN 47907, USA
[2] Department of Botany and Plant Pathology, Purdue University, West Lafayette, IN 47907, USA
[3] EMBRIO Institute, Purdue University, West Lafayette, IN 47907, USA

[*] Author for correspondence: staiger@purdue.edu

ORCID IDs: 0000-0001-9629-7133 (L.X.); 0000-0002-2906-1566 (J.L.); 0000-0003-2321-1671 (C.J.S.).

One sentence summary: Using advanced live-cell imaging along with genetic mutation and small molecule inhibitor approaches, the roles of two classes of actin filament nucleator in maintaining the homeostatic cortical cytoskeleton array are defined.

Running Title: Actin Filament Nucleation

Key words: actin cytoskeleton, Arp2/3 complex, formin, microscopy, nucleation factors, profilin

The author responsible for the distribution of materials integral to the findings presented in this article in accordance with the policy described in the Instructions for Authors is: Christopher J. Staiger (staiger@purdue.edu)

Abstract

Precise control over how and where actin filaments are created leads to the construction of unique cytoskeletal arrays within a common cytoplasm. Actin filament nucleators are key players in this activity and include the conserved Actin-Related Protein 2/3 (Arp2/3) complex, that creates dendritic networks of branched filaments, as well as a large family of formins that typically generate long, unbranched filaments and bundles. In some eukaryotic cells, these nucleators compete for a common pool of actin monomers and loss of one favors the activity of the other. To test whether this is a common mechanism, we combined the ability to image single filament dynamics in the homeostatic cortical actin array of living Arabidopsis (*Arabidopsis thaliana*) epidermal cells with genetic and/or small molecule inhibitor approaches to stably or acutely disrupt nucleator activity. We found that Arp2/3 mutants or acute CK-666 treatment markedly reduced the frequency of side-branched nucleation events as well as overall actin filament abundance. We also confirmed that plant formins contribute to side-branched filament nucleation in vivo. Surprisingly, simultaneous inhibition of both classes of nucleator increased overall actin filament abundance and enhanced the frequency of *de novo* nucleation events by an unknown mechanism. Collectively, our findings suggest that multiple actin nucleation mechanisms cooperate to generate and maintain the homeostatic cortical array of plant epidermal cells.

Introduction

The actin cytoskeleton comprises a dynamic network of filaments that participates in a wide variety of cellular activities, including vesicle/organelle trafficking, cell expansion, cellulose synthesis, tissue/organelle development, and resistance to microbial pathogen invasion (Gao et al., 2009; Sampathkumar et al., 2013; Peremyslov et al., 2015; Scheuring et al., 2016; Qi and Greb, 2017; Li and Staiger, 2018; Zhang et al., 2019). Plant cells rearrange their actin cytoskeleton organization on timescales of seconds to minutes in response to biotic or abiotic stimuli, which means the actin cytoskeleton organization is extremely dynamic but also precisely controlled (Staiger et al., 2009; Henty-Ridilla et al., 2013b). Regulation of cytoskeletal organization and dynamics involves dozens of actin-binding proteins that participate in filament nucleation, elongation, severing, and depolymerization. Nucleation factors or nucleators initiate the formation of new actin filaments at a much faster rate than spontaneous nucleation from free actin monomers and are therefore considered key regulators of array formation and actin dynamics (Kadzik et al., 2020; Rosenbloom et al., 2021). Previous in-vitro studies, primarily from non-plant systems, have identified and characterized two classes of conserved actin nucleator, the Actin-Related Protein 2/3 (Arp2/3) complex and formins, with different specific activation mechanisms (Kovar, 2006; Pollard, 2007; Paul and Pollard, 2008; Burke et al., 2014; Suarez et al., 2015).

The Arp2/3 complex is a seven-subunit protein complex responsible for generating branched actin filaments and forming dendritic actin networks in eukaryotic cells (Mullins et al., 1998; Pollard, 2007). The ARP2 and ARP3 subunits mimic the structure of actin monomers. Once the Arp2/3 complex is activated, the ARP2 and ARP3 subunits along with a recruited actin monomer serve as the actin nucleus for the polymerization of a new (daughter) filament, which grows from the side of a pre-existing (mother) actin filament with a characteristic 70° angle (Mullins et al., 1998; Dayel and Mullins, 2004; Pollard, 2007; Beltzner and Pollard, 2008; Rouiller et al., 2008). This branched actin network structure is critical for many cellular processes in yeast and animal cells, such as cell division, cell migration, exocytosis, endocytosis and tissue or embryo development (Roh-Johnson and Goldstein, 2009; Cabrera et al., 2011; Sun et al., 2013; van der Kammen et al., 2017). In contrast, plants, such as Arabidopsis, with mutations in Arp2/3 subunits have relatively normal morphology and fertility; however, *arp2/3* mutants exhibit defects in epidermal cell morphology including distorted trichomes, cell-cell adhesion defects, and fewer lobes on leaf pavement cells (Szymanski et al., 1999; Le et al., 2003; Li et al., 2003; Mathur et al., 2003a; Harries et al., 2005; Yanagisawa et

96 al., 2015). Recent research shows that the plant Arp2/3 complex is also involved in auxin
97 transport (Peng et al., 2017; Sahi et al., 2018; García-González et al., 2020), guard cell opening
98 and closing (Jiang et al., 2012; Li et al., 2014), resistance to penetration-mediated infection by
99 fungal pathogens (Qin et al., 2021), and possibly in autophagy (Wang et al., 2016; Wang et al.,
100 2019). Many of these studies reveal that *arp2/3* mutant cells have reduced actin filament
101 abundance or misaligned actin bundles, suggesting that the functions of the Arp2/3 complex
102 may be accomplished through generating specific actin structures. In growing trichome
103 branches, for example, the Arp2/3 complex generates a tip-localized actin filament array
104 constrained by cortical microtubules that coordinates growth (Yanagisawa et al., 2015;
105 Yanagisawa et al., 2018). During fungal invasion, the Arp2/3 complex localizes to the site of
106 penetration peg attack in epidermal pavement cells and generates a cortical actin filament patch
107 necessary to suppress invasion (Qin et al., 2021). However, the molecular mechanisms by
108 which the Arp2/3 complex coordinates the organization of cortical actin filament arrays in
109 unstimulated cells or how it generates unique arrays in response to biotic and abiotic stress are
110 poorly understood.

111 Formins represent another family of evolutionarily-conserved actin filament nucleators;
112 they typically generate long linear actin filaments that can bundle together to form actin cables
113 (Kovar, 2006; Pollard, 2007; Paul and Pollard, 2008). These actin cables provide tracks for
114 intracellular organelle/vesicle trafficking. Formins have two universally conserved formin-
115 homology (FH) domains, FH1 and FH2. The proline-rich FH1 domain allows formins to recruit
116 profilin-bound actin to elongate actin filaments at the barbed ends. The FH2 domain, on the
117 other hand, associates with other regions within itself for autoinhibition or it can interact with the
118 FH2 domain of another formin to form a dimer that interacts with and suitably positions two actin
119 monomers, thereby initiating the nucleation of linear actin filaments (Cvrčková et al., 2000;
120 Deeks et al., 2002; Cheung and Wu, 2004; Cvrčková et al., 2004; Kovar, 2006; Michelot et al.,
121 2006; Pollard, 2007; Paul and Pollard, 2008). There are 21 formin homologs in Arabidopsis and
122 these are separated into two phylogenetic subclasses (Cvrčková et al., 2000). Based on
123 sequence prediction, Class I formins have a signal peptide and an N-terminal transmembrane
124 domain that target them to the plasma membrane, whereas Class II formins are predicted to
125 have more diverse domain organization (Cvrčková et al., 2000; Deeks et al., 2002; Cheung and
126 Wu, 2004; Cvrčková et al., 2004; Michelot et al., 2006). In addition, plant formin orthologs can
127 be categorized according to the ability to associate with filament barbed ends and elongate
128 growing filaments. Processive formins remain attached to the actin filament barbed end and

129 move processively as the filament elongates, whereas non-processive formins remain at the
130 filament nucleation site (Cvrčková et al., 2000; Deeks et al., 2002; Cheung and Wu, 2004;
131 Cvrčková et al., 2004; Michelot et al., 2005; Michelot et al., 2006; Zhang et al., 2016).
132 Biochemical results reveal that a non-processive Class I formin, FORMIN1 (AFH1), attaches to
133 the side of a pre-existing actin filament to nucleate new filaments, suggesting a far more
134 complicated role for formins in plant cells than just the ability to generate linear filaments
135 (Michelot et al., 2006). In addition, both in-vivo and in-vitro experiments show that formins are
136 critical for maintaining homeostatic actin array organization as well as regulating polarized cell
137 growth (Vidali et al., 2009; Rosero et al., 2013; Lan et al., 2018). However, the detailed
138 molecular mechanism of how formins regulate cytoskeletal organization and single actin
139 filament dynamics in plant cells remains unclear.

140 The decision of when and where to generate an actin array as well as its specific
141 structure and dynamics is essential for each actin array to specifically choreograph its cellular
142 function and often requires coordination between the Arp2/3 complex and formins. Studies in
143 fission yeast and some animal cells indicate that the Arp2/3 complex and formins compete for a
144 limited supply of actin monomers and this competition prevents excessive activity of one or the
145 other, thereby allowing cells to generate distinct actin structures and dynamics by regulating the
146 balance of activities between these two nucleators (Hotulainen and Lappalainen, 2006; Lomakin
147 et al., 2015; Suarez et al., 2015; Davidson et al., 2018; Antkowiak et al., 2019; Chan et al.,
148 2019; Kadzik et al., 2020). During actin array assembly, the Arp2/3 complex generates
149 branched filament arrays, whereas formins produce linear filament bundles (Carlier and
150 Shekhar, 2017). Furthermore, in-vitro studies reveal that filaments generated by formins grow
151 faster than Arp2/3-nucleated filaments (Vavylonis et al., 2006; Michelot et al., 2013; Suarez et
152 al., 2015; Funk et al., 2019). Studies with M2 melanoma cells and HeLa cells illustrate that actin
153 arrays generated by different nucleators have distinct properties of filament abundance, filament
154 length, and turnover kinetics, but also reveal that both nucleators contribute to maintenance and
155 turnover of the homeostatic actin cortex (Fritzsche et al., 2016). A recent study in Arabidopsis
156 shows that actin arrays in cotyledon epidermal pavement cells are slightly more dense and the
157 extent of bundling is unchanged when either a Class I formin, AFH1, or the Arp2/3 subunit,
158 ARPC5, are genetically down-regulated; however, single filament dynamics or nucleation events
159 were not evaluated directly (Cifrová et al., 2020). The authors propose that the Arp2/3 complex
160 and formins in plants may have complementary roles to overcome the loss of the other.
161 Therefore, it is important to understand how each nucleator regulates the structure and dynamic

162 properties of actin arrays individually to better understand how they contribute to the cortical
163 actin homeostasis and how they are coordinated to regulate the actin cytoskeleton during
164 different biological processes.

165 Quantitative analysis of single actin filament dynamics in vivo is relatively hard to
166 conduct in yeast and mammalian cells, because either the cells are too small or the actin arrays
167 are too dense and filament lengths are below the limits of resolution of light microscopy.
168 Epidermal cells from dark-grown Arabidopsis hypocotyls are large in size and have relatively
169 sparse actin arrays in the cortical cytoplasm, making this a powerful model system for
170 quantitative analysis of single actin filament dynamics, especially when combined with high
171 spatial and temporal resolution imaging approaches and genetically-encoded fluorescence
172 reporters (Staiger et al., 2009; Henty et al., 2011; Henty-Ridilla et al., 2013a; Cai et al., 2014;
173 Cao et al., 2016; Arieti and Staiger, 2020). Previous work demonstrates a remarkably high rate
174 of new filament construction, rapid growth at filament ends, and disassembly by prolific severing
175 activity in a mechanism termed “stochastic dynamics” (Staiger et al., 2009). High rates of
176 polymerization are likely supported by a large pool of monomeric actin that is buffered with an
177 excess of the monomer-binding protein, profilin, to suppress spontaneous nucleation events
178 (Chaudhry et al., 2007; Staiger et al., 2009; Cao et al., 2016). The ability to observe both actin
179 filament architecture and activities of single filaments in living cells allows direct visualization
180 and quantitative analysis of the effects associated with the disruption of actin nucleators on
181 filament activities in vivo (Cao et al., 2016).

182 In this study, we test the hypothesis that the Arabidopsis Arp2/3 complex mediates
183 nucleation of side-branched filaments in vivo but does not facilitate filament elongation directly.
184 We used both genetic and pharmacological approaches to disrupt Arp2/3 complex activity in
185 plant cells. With quantitative live-cell imaging at single filament resolution, we demonstrated
186 directly that the Arp2/3 complex is responsible for the nucleation of side-branched filaments in
187 vivo. We also characterized the difference between the Arp2/3 complex and formins with
188 respect to the dynamic behaviors of the filaments they generate and evaluated the
189 consequence of losing both classes of filament nucleator on actin organization and dynamics.
190 Surprisingly, living plant cells deficient for two classes of nucleator generate comparatively
191 normal and dynamic actin arrays by an apparent *de novo* filament nucleation mechanism.

192

Results

Arabidopsis plants have defects in general growth and epidermal cell morphology when deficient for the Arp2/3 complex

Previous studies of Arp2/3 complex mutants reveal defects in Arabidopsis epidermal cell growth and morphology (Szymanski et al., 1999; Le et al., 2003; Li et al., 2003; Mathur et al., 2003b; Harries et al., 2005; Facette et al., 2015; Yanagisawa et al., 2015; Cifrová et al., 2020). Here, we acquired a T-DNA insertion mutant for *ARP2*, *arp2-1* (or *wrm1-2*; SALK_003448), and a point mutation of *ARPC2*, *arpc2* (or *dis2-1*; El-Assal et al., 2004), and confirmed the cell and organ growth phenotypes. We observed that both *arp2-1* and *arpc2* homozygous mutant plants had adhesion defects at end walls of hypocotyl epidermal cells and severely distorted leaf trichomes when compared to wild-type sibling lines (Supplemental Fig. S1A). In addition, etiolated hypocotyls from *arp2-1* and *arpc2* seedlings were significantly shorter than wild-type seedlings at the same time points (Supplemental Fig. S1, B and C). To test whether these growth defects resulted from defects in cell expansion, we examined epidermal cell length and found that cells in all regions of etiolated *arp2/3* hypocotyls were significantly shorter compared to wild-type hypocotyls; however, cell widths were not affected (Supplemental Fig. S1, D and E). Similar results for root growth were observed in light-grown seedlings (Supplemental Fig. S1, F and G). These results confirm that the Arp2/3 complex plays a role in axial cell expansion in both dark-grown hypocotyls and light-grown roots of Arabidopsis.

Actin filament abundance and bundling are reduced in *arp2/3* mutants

To assess the influence of the Arp2/3 complex on cortical actin cytoskeletal organization, we compared images of epidermal cells from the apical region of 5-d-old etiolated wild-type, *arp2-1,* and *arpc2* hypocotyls collected by variable-angle epifluorescence microscopy (VAEM) (Staiger et al., 2009). Homozygous mutant and isogenic wild-type sibling lines that express the actin reporter, green fluorescent protein (GFP) fused with FIMBRIN1 actin-binding domain 2 or GFP-fABD2 (Sheahan et al., 2004) were prepared by crossing to facilitate the observation and measurement of actin cytoskeleton organization and filament dynamics (Staiger et al., 2009). The actin array structure in *arp2-1* and *arpc2* cells had fewer, thinner, and more scattered filaments compared to corresponding wild-type cells (Fig. 1A). To compare these differences quantitively, we used *density*, *skewness* and *the coefficient of variation (CV)* as three key parameters established previously for standardized descriptions of actin cytoskeleton array organization in living cells (Higaki et al., 2010; Ueda et al., 2010; Henty et al., 2011; Higaki et

225 al., 2020). Density measures the percentage of occupancy of actin filaments in an array,
226 whereas both skewness and CV define the extent of bundling of actin filaments. CV uses a
227 different calculation method compared to skewness, and is reportedly a better indicator of
228 bundling, especially for VAEM images (Higaki et al., 2020). Actin density in *arp2-1* and *arpc2*
229 cells was significantly decreased compared to the respective wild-type cells (Fig. 1B), and the
230 extent of filament bundling was significantly reduced as well when measured by skewness or
231 CV methods (Fig. 1C and D). These results demonstrate that the Arp2/3 complex contributes to
232 the generation of both individual filaments and filament bundles and is necessary for
233 maintaining the homeostatic organization of the cortical actin cytoskeleton in epidermal cells.

234 **The Arp2/3 complex plays a significant role in filament nucleation and generation of side-**
235 **branched filaments**

236 To investigate whether the Arp2/3 complex participates in actin filament nucleation, we
237 measured single actin filament formation and dynamics in wild-type and *arp2/3* mutant cells by
238 collecting time-lapse movies from the apical regions of 5-d-old dark-grown hypocotyls with
239 VAEM. The sparse nature of the cortical actin array in hypocotyl epidermal cells and the high
240 spatial and temporal resolution afforded by VAEM allowed us to visualize (Fig. 2A) and quantify
241 individual nucleation events with a previously described assay (Cao et al., 2016). Briefly, we
242 counted all new or regrowing filaments identified in multiple 400 μm^2 regions of interest (ROI)
243 within a cell during a 100-s time-lapse movie. The nucleation frequency was normalized to the
244 average filament number within each ROI to minimize the influence of filament abundance
245 differences between ROIs and genotypes. The overall nucleation frequency in *arp2-1* cells (0.38
246 ± 0.03 events/filament/min) was significantly decreased compared to wild-type cells (0.62 ± 0.05
247 events/filament/min) (Fig. 2B; Supplemental Movie S1; Supplemental Movie S2) and coincided
248 with our observation that loss of function of the Arp2/3 complex resulted in a significant
249 reduction in filament abundance (Fig. 1B). Similar reductions in overall nucleation frequency
250 were also observed for *arpc2* compared to wild-type cells (Supplemental Fig. S2A). Next, we
251 classified nucleation events into three different subpopulations based on filament origin: *de novo*
252 from the cytoplasm; from the side of a pre-existing filament or bundle; or, from the end of a pre-
253 existing filament (Fig. 2A; Supplemental Movies S3 to S5) (Staiger et al., 2009; Henty-Ridilla et
254 al., 2013a; Cao et al., 2016). Only the side-branched nucleation frequency was significantly
255 decreased in *arp2-1* and *arpc2* cells compared to the respective wild-type sibling cells (Fig. 2C–
256 E; Supplemental Movies S1 and S2; Supplemental Fig. S2, C–E). Side-branched nucleation

events contribute about half of all new filament origins and these were reduced by 60–70% in the *arp2/3* mutants.

A previous study reports different results regarding the actin organization in *arp2/3* mutants; instead of significantly decreased filament abundance as observed here, a minor increase in actin filament density in *arpc5* cotyledon pavement cells was reported (Cifrová et al., 2020). These differences could result from the use of a different *arp2/3* complex subunit mutation, the investigation of epidermal cells from a different tissue, the choice of actin cytoskeleton reporter, or all of the above. Several previous publications show that LifeAct reduces both the actin reorganization rate and actin polymerization rate (van der Honing et al., 2011; Spracklen et al., 2014; Courtemanche et al., 2016), and displays longer and thicker filaments (Flores et al., 2019). To test which factors led to differing results between the current work and that of Cifrová et al. (2020), we conducted a direct comparison between the ability of GFP-fABD2 or GFP-LifeAct to report actin architecture and single filament dynamics in either etiolated hypocotyls (Supplemental Fig. S3) or light-grown cotyledons (Supplemental Fig. S4). Moreover, we introduced GFP-LifeAct into *arp2-1* to compare directly with the GFP-fABD2 *arp2-1* reporter line described above. Our results showed that *arp2-1* expressing either GFP-fABD2 or GFP-LifeAct had significantly lower actin filament density in the cortical array of both etiolated hypocotyl and light-grown cotyledon epidermal cells (Supplemental Fig. S3B and S4B). Similarly, overall actin filament nucleation frequency and the side-branched nucleation subclass were significantly reduced in *arp2-1* epidermal cells from both reporter lines, in either hypocotyls or cotyledons, compared to the corresponding wild-type lines (Supplemental Fig. S3, E–H; Supplemental Fig. S4, E–H). These results suggest that using GFP-fABD2 as the actin reporter, or imaging epidermal cells of the etiolated hypocotyl, are not causal for the actin phenotypes we observed in *arp2/3* mutants. Because it is beyond the scope of the current investigation, we did not seek to determine whether the previous findings are specific to the *arpc5* mutant allele used, but note that we find similar quantitative differences in actin architecture and nucleation frequency with mutations in two different subunits (*arp2-1* and *arpc2*) of the Arp2/3 complex. Considering the nature of the LifeAct marker in stabilizing actin structures and our primary goal of observing and analyzing the dynamic behaviors of single actin filaments, we used the GFP-fABD2 marker lines for the remainder of the experiments in this study.

Actin filaments generated by the Arp2/3 complex have unique dynamic properties

To understand how the Arp2/3 complex influences the dynamics of actin filaments, we tracked many dozens of individual filaments from their first appearance to complete disappearance and

290 measured several parameters that were previously established to describe actin filament
291 turnover (Fig. 3A; Table 1; Supplemental Movies S6 and S7)(Staiger et al., 2009; Henty et al.,
292 2011). Compared to wild type, the population distribution of actin filament elongation rates in
293 *arp2-1* cells was more left skewed, and the average filament elongation rate was also higher
294 (Fig. 3B; Table 1), indicating that actin filaments were growing significantly faster in *arp2-1* cells.
295 It is also obvious that there were two or three distinct populations of filament elongation rates
296 with peaks at 0.75 – 1.25, 2.0 – 2.25, and > 3 μm/s with the latter two categories becoming
297 more prevalent in *arp2-1* cells (Fig. 3B). Similar differences in overall elongation rate and fast-
298 growing filament populations were observed in *arpc2* (Supplemental Table S1; Supplemental
299 Fig. S2B). Filaments in both *arp2-1* and *arpc2* mutant cells also had significantly longer filament
300 lengths and lifetimes than the ones in respective wild-type cells (Table 1; Supplemental Table
301 S1).

302 Previous in vitro data suggest that filament ends generated by the Arp2/3 complex and
303 formins have different elongation rates; many formins are processive polymerases that use
304 profilin-actin to add monomers to growing filaments (Kovar et al., 2003; Romero et al., 2004;
305 Akin and Mullins, 2008; Zhang et al., 2016). To test whether dynamic properties of filaments
306 with different nucleation patterns are distinct from each other, we measured the full suite of
307 dynamic parameters for each population. We found that side-branched filaments in *arp2-1* cells
308 were significantly longer (Fig. 3, C–E) and filament lifetime was prolonged (Fig. 3, F–H)
309 compared to the side-branched filaments in wild-type cells; however, the severing frequency did
310 not show a significant difference between wild-type and *arp2-1* cells (Fig. 3, I–K). These
311 dynamic differences between side-branched filaments in *arpc2* mutant and wild-type sibling
312 cells were conserved (Supplemental Fig. S2, C–K).

313 Collectively, these data demonstrate that the Arp2/3 complex is responsible for
314 generating new filaments from the side of pre-existing filaments and is necessary for cells to
315 maintain the homeostatic actin cytoskeleton architecture. Moreover, Arp2/3-nucleated filaments
316 have distinct dynamic properties compared with those generated *de novo* or from the end of a
317 pre-existing filament; in particular, they grow slower and are shorter, and have reduced filament
318 lifetimes.

319 **The small molecule inhibitor CK-666 phenocopies actin-based defects in *arp2* and *arpc2***
320 **mutants**

321 Several studies report that CK-666, a small molecule inhibitor of the Arp2/3 complex that is
322 effective on yeast and animal cells (Nolen et al., 2009; Hetrick et al., 2013), phenocopies the
323 effects of *arp2/3* mutants on tomato pollen tube growth (Liu et al., 2020) and *Arabidopsis* sperm
324 nuclear migration (Ali et al., 2020), both of which depend upon the actin cytoskeleton. Moreover,
325 a recent study demonstrates that CK-666 treatment does not influence actin redistribution
326 between the basal and apical cell region in hypocotyl epidermal cells that occurs during early
327 embryo growth (Cui et al., 2023). Because the earlier studies (Liu et al., 2020; Ali et al., 2020)
328 did not directly demonstrate the effects of CK-666 on actin organization or filament nucleation, it
329 is necessary to validate whether CK-666 influences the function of the Arp2/3 complex in plant
330 cells, as a side-branched actin filament nucleator, before we use it as an effective plant Arp2/3
331 inhibitor. We hypothesized that applying CK-666 to wild-type Arabidopsis cells would inhibit the
332 Arp2/3 complex activity and mimic the *arp2/3* mutant phenotypes described above. To test the
333 effects of CK-666, we applied a dose series (0, 1, 5, 10, 50, and 100 μM) for 5 min and collected
334 snapshots of epidermal cells from the apical region of treated hypocotyls (Supplemental Fig.
335 S5). Compared to the mock treatment (0 μM), CK-666 showed a significant reduction in both
336 filament density and the extent of bundling starting at 5 μM and reached its maximum effect at
337 50–100 μM (Supplemental Fig. S5, B–D). A time-course (0, 5, 10, 30, and 60 min) of 10 μM CK-
338 666 treatment showed that 5 min was sufficient to alter actin array organization (Supplemental
339 Fig. S5, E–G). Finally, cells were able to recover normal actin array architecture from a 5 min,
340 10 μM CK-666 application after a 30-min wash out (Supplemental Fig. S5, H–J).

341 To further examine whether CK-666 phenocopies *arp2/3* mutants, we treated 5-d-old
342 etiolated hypocotyls of wild type and *arp2-1* with either DMSO (mock) solution or 10 μM CK-666
343 for 5 min and measured actin organization and single filament dynamics. Compared to DMSO-
344 treated wild-type cells, the CK-666-treated wild-type cells had significantly decreased filament
345 abundance (Fig. 4B), extent of filament bundling (Fig. 4, C and D), as well as overall nucleation
346 frequency (Fig. 2B), and these changes mirrored actin organization in DMSO-treated *arp2-1*
347 cells. Moreover, treatment of *arp2-1* with CK-666 showed no differences in terms of filament
348 organization or dynamics compared to *arp2-1* alone (Fig. 3 and 4). CK-666 treatment also
349 potently suppressed side-branched filament nucleation in wild-type cells, but not end or *de novo*
350 filament origins (Fig. 2, C–E; Supplemental Movies S1 and S8), thereby fully phenocopying the
351 effects of *arp2-1*. Finally, treatment of *arp2-1* with CK-666 did not further reduce filament side-
352 branch nucleation events, indicating that its likely mode of action is to inhibit daughter filament

353 formation from a mother filament by the Arp2/3 complex (Fig. 2D; Supplemental Movies S8 and
354 S9).

355 When we compared the CK-666 treatment of *arpc2* with its wild-type siblings, there were
356 similar changes in actin architecture and filament nucleation frequency (Supplemental Fig. S2
357 and S6). Therefore, we validated CK-666 as a small molecule inhibitor that targets the Arp2/3
358 complex and demonstrated its utility as an acute but reversible inhibitor for studying the Arp2/3
359 complex in Arabidopsis.

360 **The Arp2/3 complex and formins are both capable of nucleating side-branched actin**
361 **filaments**

362 Our previous work shows that profilin-bound actin monomers favor formin-mediated fast actin
363 filament elongation at rates > 2 μm/s (Cao et al., 2016), and the data above suggest that
364 Arp2/3-nucleated filament barbed ends elongated at intermediate rates of 1.25–1.5 μm/s (Fig.
365 3B; Supplemental Fig. S2B). We previously demonstrated the effectiveness of Small Molecule
366 Inhibitor of Formin Homology 2 (SMIFH2) in Arabidopsis both in vivo and in vitro (Cao et al.,
367 2016). The actin array organization is altered and filament nucleation frequency is significantly
368 reduced when wild-type hypocotyl epidermal cells were treated with 25 μM SMIFH2 for 5 min
369 (Cao et al., 2016), and similar results were obtained here (Fig. 5; Fig. 6, A and C–E;
370 Supplemental Movie S10).

371 To test whether the homeostatic actin filament array generated by these two nucleators
372 depends upon the Arp2/3 complex or formins, or both, we genetically and/or chemically inhibited
373 the Arp2/3 complex and formins. Both Arp2/3-inhibited (DMSO-treated *arp2-1* or *arpc2)* or
374 formin-inhibited (SMIFH2-treated wild-type) cells had a significant decrease in actin filament
375 abundance as well as in the extent of filament bundling compared to DMSO-treated wild type
376 (Fig. 5; Supplemental Fig. S7). Thus, both the Arp2/3 complex and formins are required to
377 generate dense arrays of individual actin filaments in the homeostatic actin cortex. To test
378 whether filament dynamics or the types and extent of filament nucleation are distinctly due to
379 the Arp2/3 complex or formins, we examined single filament dynamics in genetically- and/or
380 chemically- inhibited material. The nucleation frequency of both total and side-branching
381 filaments was significantly decreased in both Arp2/3-inhibited (DMSO-treated *arp2-1*) and
382 formin-inhibited (SMIFH2-treated wild-type) cells compared to wild-type (Fig. 6, A and C–E;
383 Supplemental Movies S2 and S10), and the nucleation frequency of side-branched filaments in
384 Arp2/3-inhibited cells (0.09 ± 0.01 events/filament/min) was ~45% less than in formin-inhibited

385 cells (0.16 ± 0.02 events/filament/min; Fig. 6D). However, the nucleation frequency due to *de*
386 *novo* filament origins was not influenced when either the Arp2/3 complex or formin were
387 suppressed (Fig. 6C). The average filament elongation rate in Arp2/3-inhibited cells (1.89 ± 0.07
388 μm/s) was also significantly higher than the rate in formin-inhibited cells (1.57 ± 0.06 μm/s) or in
389 wild-type cells (1.79 ± 0.05 μm/s). In addition, the population distribution of filament elongation
390 rates in Arp2/3-inhibited cells was significantly left-skewed (peak value at 2.0–2.5 μm/s)
391 compared to wild type (peak value at 1.25–1.75 μm/s), whereas formin-inhibited cells lost a
392 large portion of filaments elongating at 2.0–2.5 μm/s but the distribution had a prominent peak
393 at 1.0–1.5 μm/s (Fig. 6B). In addition, filaments in Arp2/3-inhibited cells had a longer average
394 length compared to formin-inhibited cells (Fig. 6, F–H), but we did not observe any significant
395 difference in filament lifetime or severing frequency when parameters of side-branched
396 filaments in Arp2/3-inhibited cells and formin-inhibited cells were compared (Fig. 6, I–N). Again,
397 we found similar results in both actin architecture (Supplemental Fig. S7) and single filament
398 dynamics (Supplemental Fig. S8) when *arpc2* and its respective wild-type line treated with
399 DMSO solution or SMIFH2 were compared. These data indicated that both the Arp2/3 complex
400 and formin predominantly generate side-branched actin filaments and formin-nucleated
401 filaments elongate faster and longer than Arp2/3-nucleated ones.

402 To test whether SMIFH2 exhibits off-target inhibition of myosin superfamily members, as
403 reported in Drosophila (Nishimura et al., 2021), we evaluated the influence of SMIFH2 (and CK-
404 666) on the activity of myosin XIK, the major myosin isoform mediating the delivery, vesicle
405 tethering, and exocytosis of secretory vesicles in Arabidopsis cells (Zhang et al., 2021). We
406 found that neither SMIFH2 nor CK-666 treatment reduced the speed of myosin XIK-YFP motility
407 compared to pentabromopseudilin (PBP), an effective myosin inhibitor in plant cells
408 (Supplemental Fig. S9, D–F) (Zhang et al., 2019). In addition, we also measured filament
409 convolutedness and the rate of change of convolutedness of actin filaments, which are
410 parameters describing the buckling and straightening of filaments (Staiger et al., 2009; Cai et
411 al., 2014). Both parameters were significantly decreased after treatments with SMIFH2 or PBP,
412 but unchanged by CK-666, indicating that SMIFH2 does indeed alter filament buckling and
413 straightening (Supplemental Fig. S9, A–C). These data suggest that SMIFH2 may not have an
414 off-target effect on the activity of myosins XI based on the lack of effect on the motility of YFP-
415 XIK; however, it is remains a formal possibilitythat SMIFH2 targets myosin isoforms other than
416 myosin XIK. Although the inhibition of filament buckling and straightening could indicate an off-

417 target effect of SMIFH2 on myosin XI, it seems equally likely that filament buckling is caused by
418 the processive assembly of actin filaments by Arabidopsis formins (Supplemental Fig. S9, A–C).

419 **Simultaneous genetic and/or chemical inhibition of Arp2/3 and formins increases**
420 **spontaneous filament nucleation and overall actin filament abundance**

421 To test whether two classes of nucleator cooperate to generate and maintain the homeostatic
422 actin cortical array in plant epidermal cells, we explored means to simultaneously suppress the
423 activity of both the Arp2/3 complex and formins and quantitatively evaluate the effects on actin
424 organization and dynamics. Specifically, using chemical and genetic tools to suppress the
425 activity of both the Arp2/3 complex and formins simultaneously, we applied SMIFH2 to *arp2-1 or*
426 *arpc2* cells, treated wild-type cells with a combination of CK-666 and SMIFH2, and applied CK-
427 666 to the *fh1-2* mutant. Since the Arp2/3 complex and formins are, so far, the only two actin
428 filament nucleators identified in plant cells, we predicted that simultaneously inhibiting the
429 Arp2/3 complex and formin would markedly suppress actin filament nucleation activities and
430 significantly reduce filament abundance. Surprisingly, in *arp2-1* cells treated with SMIFH2, the
431 actin filament abundance was significantly increased compared to cells with normal Arp2/3
432 complex and formin activities or with only one nucleator inhibited (Fig. 5B). Notably, SMIFH2-
433 treated *arp2-1* cells exhibited a marked abundance of short, single actin filaments in the cortical
434 array (Fig. 5A). Unlike actin array density, the extent of actin filament bundling was not restored
435 to wild-type levels when both the Arp2/3 complex and formins were simultaneously inhibited
436 (Fig. 5, C and D). In addition to increased filament abundance, total filament nucleation
437 frequency was significantly increased when both the Arp2/3 complex and formin activities were
438 reduced, and a 2.5-fold enhancement of *de novo* filament origins was responsible for this
439 increase (Fig. 6, A and C–E; Supplemental Movie S11). However, the lengths of filaments
440 generated *de novo* or from the side-branching nucleation events were both significantly reduced
441 in SMIFH2-treated *arp2-1* cells compared to other treatments and genotypes (Fig. 6, F–H).
442 Similar results were obtained when *arp2-1* epidermal cells from light-grown cotyledons were
443 treated with SMIFH2 (Supplemental Fig. S4), demonstrating that enhanced filament abundance
444 and a 2.5-fold increase in *de novo* filament nucleation were not unique to etiolated hypocotyls.
445 Moreover, the findings were identical when GFP-LifeAct was used as the reporter instead of
446 GFP-fABD2 (Supplemental Fig. S3), indicating that the reporter plays little or no role in the
447 results obtained. Finally, we also observed similar phenotypes in both actin architecture and
448 filament dynamics when we applied SMIFH2 to *arpc2* (Supplemental Fig. S7 and S8) or
449 simultaneously applied CK-666 and SMIFH2 to wild type (Fig. 7). These results indicate that a

450 marked increase in *de novo* filament nucleation results when both the Arp2/3 complex and
451 formins are inhibited in plant epidermal cells.

452 Beside the possible inhibition of myosin XI, another potential issue with using SMIFH2
453 as a formin inhibitor on plant cells is that Arabidopsis has 21 FORMIN homologs, and it remains
454 unclear whether SMIFH2 can inhibit all of them. To investigate the efficacy of SMIFH2 for
455 suppressing formin activity, as well as its ability to phenocopy the effects of plant formin
456 mutants, we prepared a homozygous *AtFORMIN1* mutant line, *fh1-2*, expressing GFP-fABD2.
457 AtFORMIN1 is a major housekeeping formin homolog in Arabidopsis vegetative tissues
458 (Cvrčková et al., 2000; Blanchoin and Staiger, 2010; Rosero et al., 2013; Rosero et al., 2016).
459 Previously, we demonstrated that SMIFH2 inhibits the nucleation and assembly activity of
460 recombinant FH2 domain from AtFORMIN1 in vitro (Cao et al., 2016). Here, we found that the
461 density of actin filament arrays was significantly reduced but the extent of filament bundling was
462 higher in DMSO-treated *fh1-2* cells compared to DMSO-treated wild-type (Fig. 8, A–D). The
463 nucleation frequency, specifically the side-branched filament subclass, was also significantly
464 decreased in DMSO-treated *fh1-2* cells compared to DMSO-treated wild-type (Fig. 8, E–H).
465 SMIFH2 treatment caused an additional reduction in both actin filament abundance and
466 nucleation activity in *fh1-2* cells (Fig. 8). These results suggest that SMIFH2 targets more formin
467 homologs than just AtFORMIN1; however, we cannot rule out the possibility that SMIFH2 does
468 not inhibit all formins. Consistent with previous biochemical results (Michelot et al., 2007), these
469 findings provide genetic evidence that AtFORMIN1 is a filament nucleator that generates new
470 daughter filaments from the side of a mother filament or bundle.

471 To further test whether loss of a single formin homolog could recapitulate the effects of
472 SMIFH2, we treated *fh1-2* with CK-666 or a combination of CK-666 and SMIFH2, as shown in
473 Figure 8. Treatment of *fh1-2* with CK-666 led to a further significant reduction in filament density
474 (Fig. 8B) as well as side-branched nucleation frequency (Fig. 8G), but no change in *de novo*
475 nucleation events (Fig. 8F), compared to DMSO-treated *fh1-2*. This does not resemble the dual
476 inhibition of wild-type with SMIFH2 and CK-666 (Fig. 7), suggesting that loss of a single major
477 formin is not responsible for the phenotype. Further, we found that identical to wild-type cells
478 simultaneously treated with SMIFH2 and CK-666, *fh1-2* responds to dual inhibition with
479 significantly increased filament abundance (Fig. 8B) as well as enhanced total (Fig. 8E) and *de*
480 *novo* nucleation frequency (Fig. 8F). These results indicate that loss of AtFH1 does not play a
481 role in the rapid response to inhibition of two classes of nucleator in epidermal cells resulting in
482 enhanced filament formation through *de novo* nucleation.

483 **PROFILIN1 does not play a role in the enhanced *de novo* nucleation in response to**
484 **simultaneous inhibition of two classes of nucleator**

485 Profilins are actin monomer-binding proteins that suppress spontaneous nucleation, prevent
486 subunit addition onto filament pointed ends (Cao et al., 2016; Sun et al., 2018), and are
487 reportedly present at up to a 3-fold molar excess to total actin protein in several plant tissues
488 (Chaudhry et al., 2007). To test whether the enhanced *de novo* actin filament nucleation, when
489 the Arp2/3 complex and formins are both inhibited, was due to spontaneous nucleation, we
490 introduced a PROFILIN1 (PRF1) mutant, *prf1-2*, to suppress one of the major profilin homologs
491 in Arabidopsis vegetative tissues (Sun et al., 2018; Qiao et al., 2019). Consistent with our
492 previous findings (Cao et al., 2016), *prf1-2* had significantly reduced actin filament abundance
493 (Fig. 9, A and B), decreased total and side-branched nucleation (Fig. 9, E and G), but modestly
494 elevated *de novo* nucleation frequency (Fig. 9F) compared to mock-treated wild type. If the
495 enhanced *de novo* nucleation frequency following simultaneous inhibition of both nucleators is
496 due to the spontaneous nucleation resulting from increased free actin monomers, then we
497 expect that *prf1-2* would be less responsive to these conditions as it presumably already has an
498 elevated free monomer concentration. We found that the triple inhibition of Arp2/3, formins and
499 PRF1 caused a significantly increased actin density (Fig. 9, A and B), as well as enhanced total
500 and *de novo* nucleation frequency (Fig. 9, E–H), all of which were slightly elevated compared
501 with dual-inhibitor treated wild type. However, either CK-666 or SMIFH2 single inhibitor
502 treatment on *prf1-2* did not cause a 2.5-fold higher *de novo* nucleation frequency (Fig. 9E) as
503 observed in dual-inhibitor treated *prf1-2* cells. These results suggest that a change in free actin
504 monomer concentration or the function of PRF1 are not the cause of the elevated *de novo*
505 nucleation when both the Arp2/3 complex and formins are inhibited.

506
507

508 **Discussion**

509 In this study, we utilized a combination of genetic mutations or small molecule inhibitors along
510 with high spatiotemporal resolution fluorescence microscopy to demonstrate, for the first time,
511 that the Arp2/3 complex nucleates side-branched actin filaments in living Arabidopsis epidermal
512 cells. We found that the Arp2/3 complex mutants, *arp2-1* and *arpc2*, had a dramatically reduced
513 overall abundance of actin filaments in the cortical array, a reduction in the extent of filament
514 bundles, and a significantly decreased frequency of side-branched nucleation events. In
515 addition, acute treatment of wild-type plants with CK-666 phenocopied the actin-based defects
516 observed in *arp2/3* mutants, whereas applying CK-666 to *arp2/3* mutants did not have any
517 additional effect on overall actin structure or filament dynamics. Thus, we confirmed that these
518 actin-based defects correlated with the loss of functional Arp2/3 complex and established that
519 CK-666 is an effective tool for inhibition of the Arp2/3 complex in plant cells. Through
520 experiments comparing genetic and chemical inhibition of the Arp2/3 complex or formins, we
521 observed that both proteins were capable of nucleating side-branched actin filaments, but that
522 Arp2/3-nucleated filaments grew slower and were shorter than formin-nucleated ones.
523 Surprisingly, simultaneous inhibition of both the Arp2/3 complex and formins led to an increase
524 in actin filament abundance and dramatically promoted *de novo* nucleation events. By
525 examining the consequences of the loss of a major housekeeping profilin isoform, PRF1, we
526 rule out the role of this monomer-binding protein in the enhanced *de novo* nucleation following
527 simultaneous inhibition of two classes of nucleator. These observations indicate that the
528 regulatory mechanisms for actin filament nucleation in the homeostatic cortical array of plant
529 cells may be unique and reveal a default response that maintains filament abundance and
530 dynamics when both nucleators are inactivated.
531

532 **The Arp2/3 complex is a major nucleator of side-branched actin filaments in *Arabidopsis***
533 **epidermal cells**

534 Biochemical studies demonstrate that the Arp2/3 complex and formins use different molecular
535 mechanisms to overcome the rate-limiting step for filament formation, and they typically
536 generate different types of actin arrays. After creating an actin nucleus, the Arp2/3 complex
537 remains attached to the pointed end of the new filament so that the barbed end is free for the
538 addition of actin monomers, profilin-actin, or capping protein (Mullins et al., 1998; Amann and
539 Pollard, 2001; Fujiwara et al., 2002; Ichetovkin et al., 2002; Rouiller et al., 2008). In contrast,

540 many formins remain associated at the filament barbed end after the nucleation, and
541 processively facilitate filament elongation through the addition of profilin-actin. This allows
542 formin-associated filaments to grow much faster and longer compared to filaments with free
543 barbed ends that are typically bound by heterodimeric capping protein (CP) soon after initiation
544 (Kovar and Pollard, 2004; Romero et al., 2004; Kovar, 2006). Based on these observations, the
545 conventional model of actin nucleation posits that formins generate long, unbranched filaments
546 with a fast filament elongation rate, whereas the Arp2/3 complex nucleates short, branched
547 actin networks with a slower growth rate. The Arp2/3 complex is accepted as a major nucleator
548 of side-branched actin filaments in yeast and animal cells (Mullins et al., 1998; Amann and
549 Pollard, 2001; Fujiwara et al., 2002; Ichetovkin et al., 2002; Rouiller et al., 2008). Even though
550 the Arp2/3 complex is also shown to be critical for plant cells to maintain their homeostatic actin
551 organization and is required for a wide variety of cellular activities, little is known about the exact
552 function of plant Arp2/3 complex in terms of its contribution to actin filament dynamics.

553 In this study, we characterized the function of the Arp2/3 complex in coordinating the
554 organization of the cortical actin array as well as single actin filament dynamics in living
555 Arabidopsis cells. Epidermal cells of etiolated hypocotyls, as well as light-grown cotyledons, with
556 genetically- or chemically-inhibited Arp2/3 complex showed a quantifiable decrease in both actin
557 filament abundance and extent of filament bundling, and, more importantly, there was a
558 significantly reduced nucleation frequency of side-branched actin filaments. Branched filament
559 formation represents more than half of all nucleation events in the cortical actin array of
560 hypocotyl or cotyledon epidermal cells, and these were reduced by 50–70% when the Arp2/3
561 complex was inhibited chemically or genetically. These results suggest that the Arp2/3 complex
562 is a major nucleator of side-branched actin filaments in Arabidopsis epidermal cells. Our data
563 also provide a compelling live-cell view of the formation of branched actin filaments by active
564 Arp2/3 complex at single filament resolution. Furthermore, our results reveal that there are at
565 least two populations of filaments with different dynamic properties, likely due to different
566 filament growth mechanisms and/or the availability of filament barbed ends for monomer
567 addition, that contribute to the organization of the homeostatic actin cortical array in epidermal
568 cells. By examining filament elongation rate frequencies when formin activity was suppressed,
569 or when both the Arp2/3 complex and formins were inhibited, filaments with elongation rates of
570 1–1.25 μm/s predominated. We expect this represents the population of filaments with free
571 barbed ends extending by monomer addition and is consistent with the in-vitro mechanism of
572 branched filament nucleation by the Arp2/3 complex.

573

574 **The Arp2/3 complex and formins both mediate side-branched filament nucleation but**
575 **generate filaments with unique dynamic properties**
576 Nucleation is the rate-limiting step for actin filament formation in vitro and depends on the
577 availability of actin monomers and is suppressed by profilin (Pollard et al., 2000; Sept and
578 McCammon, 2001; Michelot et al., 2005). Previous results with the fission and budding yeasts,
579 *Schizosaccharomyces pombe* and *Saccharomyces cerevisiae*, as well as mammalian cells
580 reveal a competition between the Arp2/3 complex and formin for a limited pool of actin
581 monomers; consequently, formin-mediated long filament bundles dominate when the Arp2/3
582 complex is inhibited, whereas an increased abundance of actin patches created by the Arp2/3
583 complex are prominent when formin is down-regulated (Hotulainen and Lappalainen, 2006;
584 Burke et al., 2014; Lomakin et al., 2015; Suarez et al., 2015; Fritzsche et al., 2016; Davidson et
585 al., 2018; Antkowiak et al., 2019; Chan et al., 2019; Kadzik et al., 2020). Plant cells, by contrast,
586 appear to show cooperation between these two nucleators rather than a competition to build
587 distinct actin arrays. The cortical cytoplasm of epidermal cells contains a dynamic actin array
588 that is rather disordered and comprises comingled actin filament bundles and individual actin
589 filaments (Staiger et al., 2009; Smertenko et al., 2010). Evidence for actin patches or dense
590 dendritic actin networks is limited to certain cell types, such as guard mother cells (Facette et
591 al., 2015), the apex of trichomes (Yanagisawa et al., 2015), or at focal sites elicited by pathogen
592 attack (Hardham et al., 2007; Qin et al., 2021). Our results revealed that the density of actin
593 filaments in the cortical array, the extent of filament bundling, as well as filament nucleation
594 frequency all decreased when either the Arp2/3 complex or formins were inhibited, suggesting
595 that the Arp2/3 complex or formins alone are not able to maintain the homeostasis of the cortical
596 actin arrays when the other nucleator is not functional. These results indicate that plant cells
597 may have a different actin regulatory mechanism for constructing actin filament arrays
598 compared to yeast or some animal cells. Our results are consistent with a previous report
599 showing partial cooperation between plant filament nucleation mechanisms in Arabidopsis
600 cotyledon epidermal cells, however, the consequences of losing either class of nucleator were
601 markedly different (Cifrová et al., 2020). That study showed a minor increase in actin filament
602 density in either the formin *fh1* mutant or the *arpc5* mutant (Cifrová et al., 2020), rather than the
603 prominent decreases observed here. As demonstrated here, these differences are not due to
604 the use of different actin filament reporters (LifeAct versus fABD2), different developmental state
605 and organ for examining epidermal cells (cotyledons versus dark-grown hypocotyls), or the

606 result of compensation from genetic loss of one formin isoform versus acute treatment with a
607 chemical inhibitor.

608 Our results showed that both the Arp2/3 complex and formins, including AtFORMIN1,
609 are responsible for generating side-branched filaments because the inhibition of either one led
610 to a significant reduction in side-branched filament nucleation and did not promote the other two
611 subclasses of filament nucleation. These results also suggest that the Arp2/3 complex and
612 formins are not competing for actin monomers for filament nucleation. Based on the total actin
613 concentration, the ratio of F-actin to total actin, and the ratio of profilin to total actin in other plant
614 tissues, the estimated actin monomer pool in Arabidopsis hypocotyl cells is relatively large and
615 most monomers are likely to be in a profilin-actin complex (Chaudhry et al., 2007; (Staiger et al.,
616 2010); therefore, the Arp2/3 complex and formins may not have to compete for a limited supply
617 of actin monomers in plant cells. Here, if we assume that 1.25 μm/s is the rate of addition of
618 monomers to free barbed ends, that the association rate constant for plant actin is similar to
619 ATP-loaded rabbit skeletal muscle α-actin (k_+ = 11.6 μM^{-1} s^{-1}) and that a micron of actin filament
620 comprises 370 subunits (Pollard et al., 2000), then we estimate the available monomer pool to
621 be 40 μM in hypocotyl epidermal cells using the equation: [G-actin] = rate/k_+. In addition, even
622 though both the Arp2/3 complex and formins generate side-branched actin filaments, these
623 filaments have markedly different properties. We found that formin-nucleated filaments grew
624 significantly faster at rates of 2–2.25 μm/s, with another small subpopulation growing at rates >
625 3 μm/s. The different properties of filament barbed ends as well as a large pool of monomers,
626 perhaps buffered with profilin, may facilitate the fast-growing filaments nucleated by side-
627 branching as previously found in Arabidopsis cells (Cao et al., 2016), and is consistent with
628 previous in vitro results (Vavylonis et al., 2006; Michelot et al., 2013; Suarez et al., 2015; Zhang
629 et al., 2016; Funk et al., 2019).

630 If using the conventional model for how formins generate new actin filaments, we would
631 predict that plant processive formins not only generate growing filaments from the side of a
632 mother filament but also remain attached to the barbed end of the new filament to facilitate the
633 addition of profilin-actin to the growing ends, resulting in faster and longer side-branched
634 filaments compared to Arp2/3-nucleated ones. However, previous in vitro data showed that the
635 AtFORMIN1 nucleates actin filaments but remains associated at the pointed end and does not
636 compete with capping protein for filament barbed ends, indicating it is non-processive and
637 associates with the side of filaments after nucleation (Michelot et al., 2006). Further, SMIFH2

638 application in our studies reduced nucleation frequency but did not reduce the filament length of
639 side-branched filaments compared to the mock treatment. Both in vitro and in vivo results
640 suggest that non-processive formins in plant cells may have a weak interaction with filament
641 barbed ends so that these formins move away from the end of the filament to its side to
642 generate a new side-branched filament instead of occupying the barbed end and facilitating
643 filament elongation. However, another in vitro analysis showed that the processive formin,
644 AtFORMIN14, promotes *de novo* filament growth via the association with profilin (Zhang et al.,
645 2016), and there are 21 FORMIN homologs in *Arabidopsis* (Cvrčková et al., 2004; Blanchoin
646 and Michelot, 2012; Cvrčková, 2013). All these results suggest that plant formins that nucleate
647 side-branched filaments may have distinct molecular properties compared to formins that
648 nucleate *de novo* filament formation or formins found in yeast or animal cells. With the exception
649 of enhanced bundling, the loss of a single formin isoform, *fh1-2*, recapitulates but is less
650 dramatic than the effects of SMIFH2 treatment of epidermal cells supporting the conclusion that
651 multiple formin isoforms are likely inhibited by this small molecule.

652 Since SMIFH2 shows off-target inhibition of members of the myosin superfamily
653 (Nishimura et al., 2021), we were compelled to critically evaluate the effects of SMIFH2
654 treatment on plant cells. Although our data showed that SMIFH2 treatment did not influence the
655 motility of myosin XIK, it did significantly reduce filament convolutedness and the rate of change
656 of convolutedness of actin filaments, suggesting that SMIFH2 alters filament buckling and
657 straightening. However, the change in filament buckling could be the consequence of different
658 filament growth rates and processive elongation by formins (Staiger et al., 2009; Cai et al.,
659 2014; Cao et al., 2016). Even though a recent in vitro study reveals that SMIFH2 is a pan-
660 inhibitor for all human formins (Orman et al., 2022), we should not exclude the possibility that
661 SMIFH2 can only inhibit a subset of plant formin homologs. Further genetic and biochemical
662 analyses should be designed to dissect the interaction between SMIFH2 and different formin
663 homologs to determine the specificity of this chemical inhibitor on plant formins.

664

665 **Simultaneous inhibition of the Arp2/3 complex and formins promotes *de novo* nucleation**
666 **events**

667 When we combined genetic and chemical methods to downregulate the Arp2/3 complex and
668 formins simultaneously, surprisingly, the frequency of actin filament nucleation was significantly
669 enhanced by up to 2.5-fold, with *de novo* nucleation events appearing to be the exclusive
670 contributor to this enhancement. The Arp2/3 complex and formins are, to date, the only two

671 *bona fide* actin filament nucleators in plant cells (Blanchoin and Staiger, 2010; Vaškovičová et
672 al., 2013; Yanagisawa et al., 2013). Theoretically, when both the Arp2/3 complex and formins
673 are inhibited, the concentration of free actin monomers is predicted to increase but the ratio of
674 F- to G-actin and the proportion of profilin-actin in the monomer pool should both decrease. It is
675 possible that these changes in the actin monomer pool could increase the nucleation rate of
676 spontaneous filament formation thereby enhancing the total frequency of *de novo* nucleation
677 events. In support of this model, disruption of AtPRF1 led to a modest increase in *de novo*
678 nucleation events and a decrease in side-branched events (Cao et al., 2016). However, the
679 *prf1-2* mutant exhibits a 2.5-fold increase in *de novo* nucleation frequency, just like wild-type
680 epidermal cells, when both nucleators are inhibited with chemicals. Perhaps, as suggested by
681 Sun et al. (2018), another profilin isoform, PRF3, is the major regulator of spontaneous filament
682 nucleation and sequesters actin monomers that are poorly utilized by formins. The acute
683 chemical inhibition of nucleation machinery could lead to rapid post-translational modification
684 and inactivation of PRF3, thereby facilitating spontaneous filament formation from free
685 monomers. This hypothesis needs to be tested through future experiments.

686 In conclusion, our results provide direct evidence to demonstrate that the Arp2/3
687 complex nucleates side-branched actin filaments in living plant cells. These studies also confirm
688 that some formin isoforms, including AtFORMIN1, generate side-branched actin filaments in
689 plant cells, which is a unique actin filament nucleation mechanism compared to yeast or animal
690 cells. Moreover, we find that Arp2/3- and formin-nucleated filaments have distinct dynamic
691 properties, which can be applied to future studies about how cells coordinate these two
692 nucleators to regulate the actin structure and dynamics for different cellular activities. The
693 simultaneous inhibition of both the Arp2/3 complex and formin surprisingly caused an enhanced
694 *de novo* filament nucleation, which raises the possibility for a unique actin nucleation
695 mechanism to generate dynamic cortical actin arrays in plant cells.

696

697 ## Materials and methods

698 ### Plant materials and growth conditions

699 All Arabidopsis (*Arabidopsis thaliana*) plants in this study were in Columbia-0 (Col-0)
700 background. The *ARP2* T-DNA insertion line, *arp2-1* (SALK_003448), the *PRF1* T-DNA
701 insertion line, *prf1-2* (SALK_057718; Cao et al., 2016), and the *AtFORMIN1* T-DNA insertion
702 line, *fh1-2* (SALK_009693; Rosero et al., 2013) were obtained from the Arabidopsis Biological
703 Resource Center (Ohio State University). The *ARPC2* point mutation line, *arpc2* (G1217A), was
704 kindly provided by Dan Szymanski (Purdue University). Mutant lines, *arp2-1, arpc2* and *prf1-2*,
705 were crossed to wild-type (Col-0) expressing the GFP-fABD2 reporter (Sheahan et al., 2004;
706 Staiger et al., 2009) and homozygous mutants and corresponding wild-type siblings were
707 recovered from F2 populations. For the *fh1-2* line, homozygous plants were transformed with a
708 *35S::GFP-fABD2* construct using the floral dip method and seeds were screened with
709 kanamycin (Clough and Bent, 1998; Sheahan et al., 2004). For lines carry GFP-LifeAct, both
710 Col-0 and *arp2-1* mutant were transformed with a *UBQ::GFP-LifeAct* construct (kindly provided
711 by Weibing Yang from The Sainsbury Laboratory, University of Cambridge, Cambridge, UK)
712 using the floral dip method and transformants selected with BASTA (Clough and Bent, 1998).

713 Seeds were surface sterilized and stratified at 4°C for 3 days on plates comprising half-
714 strength Murashige and Skoog (MS) medium supplemented with 1% (w/v) sucrose and 1%
715 (w/v) agar. For dark-grown hypocotyl growth, seedlings were grown in continuous darkness
716 after exposing the plates to light for 4 h. For light-grown root and cotyledon growth, seeds were
717 grown vertically on plates comprising half-strength MS medium supplemented with 0% (w/v)
718 sucrose and 0.6% (w/v) agar under long-day conditions (16 h light/8h dark) at 21°C.

719 ### Drug treatments

720 For short-term live cell treatments, individual seedlings were treated for 5 min in inhibitor
721 solution in 6-well plates in the dark prior to each imaging session. Hypocotyls were mounted in
722 the inhibitor solution and imaged immediately. CK-666 (Sigma-Aldrich; Cat # 182515; St. Louis,
723 MO, USA), SMIFH2 (Sigma-Aldrich; Cat # 344092) and PBP (Adipogen; Cat # BVT-0441) were
724 dissolved in DMSO to prepare a 5 mM stock solution.

725 ### Live cell imaging

726 For both snapshot and time-lapse image acquisitions in dark grown hypocotyls, epidermal cells
727 from the apical region of 5-d-old dark-grown hypocotyls were used. In some experiments, the
728 lipophilic dye, FM4-64 (Invitrogen; Cat # T3166; Carlsbad, CA, USA), was dissolved in DMSO
729 and used at 20 mM to label the plasma membrane. All images and movies were collected using
730 variable-angle epifluorescence microscopy (VAEM) with an Olympus TIRF objective (60X, 1.45
731 numerical aperture) using SlideBook software (version 5.5; Intelligent Imaging Innovations) as
732 described previously (Staiger et al., 2009; Henty et al., 2011; Li et al., 2012; Cai et al., 2014;
733 Cao et al., 2016).

734 For experiments with cotyledons, adaxial epidermal cells from 5-d-old light-grown
735 cotyledons were used. An Olympus IX-83 microscope mounted with a spinning-disc confocal
736 unit (Yokogawa CSUX1-A1) and an Andor iXon Ultra 897BV EMCCD camera were used to
737 acquire snapshot and time-lapse images with an Olympus UPlanSApo oil objective (100X, 1.45
738 numerical aperture). GFP fluorescence was excited with a 488nm laser line and emission
739 collected through the 525/30 nm filter to visualize actin filaments. All images were collected with
740 MetaMorph software (version 7.8.8.0) as described previously (Cao et al., 2022).

741 A double-blinded experimental design was used for all image collection, processing and
742 quantitative analyses.

743 **Image processing and quantitative analysis of actin cytoskeleton architecture and single**
744 **actin filament dynamics**

745 Images and movies were processed with Fiji is Just Image J (Schindelin et al., 2012). All images
746 used for actin architecture analysis were collected with a fixed exposure time, laser power, and
747 camera gain setting.

748 To quantify actin architecture, three parameters, *density*, *skewness* and *coefficient of*
749 *variation (CV)*, were employed in this study; density measures the percentage of occupancy of
750 GFP signal in an image and skewness and CV measure the extent of actin filament
751 bundling(Higaki et al., 2010; Ueda et al., 2010; Henty et al., 2011; Li et al., 2012; Cai et al.,
752 2014; Cao et al., 2016; Arieti and Staiger, 2020). Micrographs were analyzed in Fiji Is Just
753 Image J using the methods described previously (Higaki et al., 2010; Henty et al., 2011; Li et al.,
754 2012; Higaki et al., 2020).

755 To compare single actin filament parameters between genotype or drug treatment,
756 double-blind experiments (data collection and analysis) were performed. Maximum filament
757 length and lifetime, filament severing frequency, elongation rates, filament convolutedness and
758 the rate of change of convolutedness were measured as described previously (Staiger et al.,
759 2009; Henty et al., 2011; Li et al., 2012; Cai et al., 2014; Cao et al., 2016). For nucleation
760 frequency analysis, a 400 μm^2 ROI was randomly selected from movies of epidermal cells at the
761 apical region of the hypocotyl, and all observable nucleation events were counted during a time
762 period of 100 s, according to Cao et al., 2016. To account for differences in filament density in
763 genotypes or drug treatments, the nucleation frequency was normalized against filament
764 numbers in each ROI.

765 For actin architecture analysis in both hypocotyl and cotyledon epidermal cells, more
766 than 150 ROIs were selected from 50 images of cells collected from at least 10 individual
767 seedlings per genotype or treatment. For nucleation frequency analysis, more than 300 events
768 from at least 10 individual seedlings were observed per genotype or treatment. For single actin
769 filament dynamics analysis, at least 5 newly-appeared filaments were tracked from their first
770 appearance to their complete disappearance in each hypocotyl, and more than 50 filaments
771 from at least 10 hypocotyls were measured per genotype or treatment. For all statistical
772 comparisons and plotting, the average value from a single hypocotyl was used as one data
773 point. All experiments were conducted with at least 2 independent biological repeats to make
774 conclusions in each figure.

775 **Statistical analyses**

776 Two-way ANOVA with Tukey's post-hoc tests were performed in SPSS (version 25) to
777 determine the significance among different genotypes/treatments. Chi-square tests were
778 performed for statistically comparing parametric distributions and P values were calculated in
779 Excel 15.32. Any difference with a P value less than 0.05 was considered significantly different.
780 Detailed statistical analysis data are shown in Supplemental Data Set 1.

781 **Supplemental data**

782 The following materials are available in the online version of this article.

783 **Supplemental Table S1.** Single actin filament dynamics in wild type (*ARPC*2) and *arpc2* mutant
784 with or without CK-666.
785 **Supplemental Figure S1.** Disruption of the Arp2/3 complex perturbs epidermal cell morphology
786 and inhibits normal plant growth.
787 **Supplemental Figure S2.** Actin filament nucleation frequency is decreased in *arpc2* and after
788 treatment of wild type with CK-666.
789 **Supplemental Figure S3.** Two different actin cytoskeleton markers, GFP-fABD2 and GFP-
790 LifeAct, report similar changes in actin array organization and nucleation events regardless of
791 the genotype or treatment.
792 **Supplemental Figure S4.** Cotyledon epidermal cells show similar phenotypes of reduced actin
793 filament abundance and decreased nucleation frequency in *arp2-1* mutants expressing either
794 GFP-fABD2 or GFP-LifeAct cytoskeletal reporters.
795 **Supplemental Figure S5.** CK-666 is an acute and reversible chemical inhibitor of the Arp2/3
796 complex in plant cells.
797 **Supplemental Figure S6.** Actin array architecture is perturbed in *arpc2* and the reduced
798 filament density and bundling phenotypes are recapitulated by treatment with CK-666.
799 **Supplemental Figure S7.** Actin filament density increases after treatment of *arpc2* with the
800 formin inhibitor SMIFH2.
801 **Supplemental Figure S8.** Overall and *de novo* filament nucleation increase when ARPC2 and
802 formin activity are simultaneously inhibited.
803 **Supplemental Figure S9.** Filament convolutedness decreases when formin or myosin activities
804 are inhibited.**Supplemental Movie S1.** Full time-lapse sequence of actin filament nucleation
805 activities in mock-treated wild-type (*ARP2*) cells.
806 **Supplemental Movie S2.** Full time-lapse sequence of actin filament nucleation activities in
807 mock-treated *arp2-1* cells.
808 **Supplemental Movie S3.** Representative actin filament nucleated *de novo* from the cytoplasm
809 (as in Figure 3 A, top row).
810 **Supplemental Movie S4.** Representative actin filament nucleated from the side of a pre-
811 existing filament (as in Figure 3 A, middle row).
812 **Supplemental Movie S5.** Representative actin filament nucleated from the end of a pre-existing
813 filament (as in Figure 3 A, bottom row).
814 **Supplemental Movie S6.** Representative example of filament elongation (as in Figure 4 A).
815 **Supplemental Movie S7.** Representative example of filament severing (as in Figure 4 A).
816 **Supplemental Movie S8.** Full time-lapse sequence of actin filament nucleation activities in CK-
817 666-treated wild-type (*ARP2*) cells.
818 **Supplemental Movie S9.** Full time-lapse sequence of actin filament nucleation activities in CK-
819 666-treated *arp2-1* cells.
820 **Supplemental Movie S10.** Full time-lapse sequence of actin filament nucleation activities in
821 SMIFH2-treated wild-type (*ARP2*) cells.

822 **Supplemental Movie S11.** Full time-lapse sequence of actin filament nucleation activities in
823 SMIFH2-treated *arp2-1* cells.
824 **Supplementary Data Set S1.** ANOVA and Chi-square test results and parameters.
825

Acknowledgments

We thank Hongbing Luo (Purdue University) for excellent care and maintenance of plant materials, Dan Szymanski (Purdue University) for providing the *arpc2* line, and David Kovar (University of Chicago) and Laurent Blanchoin (Interdisciplinary Research Institute of Grenoble) for helpful comments on the manuscript. We are also grateful to the Arabidopsis Biological Resource Center (Ohio State University) for supplying the *arp2-1, prf1-2, and fh1-2* T-DNA insertion lines. The TIRF microscopy facility was supported, in part, by the Bindley Bioscience Center at Purdue University. This work was funded by a grant from the Physical Biosciences program of the US Department of Energy, Office of Basic Energy Sciences (DE-FG02-09ER15526) to C.J.S. Conceptualization of experiments, data analysis, and manuscript preparation by C.J.S. were also supported by the EMBRIO Institute, an NSF-Biological Integration Institute under contract no. 2120200.

The authors declare no competing financial interests.

Author Contributions

L.X. acquired and analyzed data, prepared figures, wrote and revised the manuscript; L.C. acquired and analyzed data; J.L. acquired and analyzed data; C.J.S. conceptualized experiments, acquired funding, analyzed data, wrote and revised the manuscript.

845 ## References

846 **Akin O, and Mullins RD.** Capping protein increases the rate of actin-based motility by
847 promoting filament nucleation by the Arp2/3 complex. Cell. 2008:**133**(5): 841-
848 851.10.1016/j.cell.2008.04.011
849 **Ali MF, Fatema U, Peng X, Hacker SW, Maruyama D, Sun M-X, and Kawashima T.** ARP2/3-
850 independent WAVE/SCAR pathway and class XI myosin control sperm nuclear migration
851 in flowering plants. Proc. Natl. Acad. Sci. USA. 2020:**117**(51): 32757-
852 32763.10.1073/pnas.2015550117
853 **Amann KJ, and Pollard TD.** Direct real-time observation of actin filament branching mediated
854 by Arp2/3 complex using total internal reflection fluorescence microscopy. Proc. Natl.
855 Acad. Sci. USA. 2001:**98**(26): 15009-15013.10.1073/pnas.211556398
856 **Antkowiak A, Guillotin A, Boiero Sanders M, Colombo J, Vincentelli R, and Michelot A.** Sizes of
857 actin networks sharing a common environment are determined by the relative rates of
858 assembly. PLoS Biol. 2019:**17**(6): e3000317.10.1371/journal.pbio.3000317
859 **Arieti RS, and Staiger CJ.** Auxin-induced actin cytoskeleton rearrangements require AUX1. New
860 Phytol. 2020:**226**(2): 441-459.10.1111/nph.16382
861 **Beltzner CC, and Pollard TD.** Pathway of actin filament branch formation by Arp2/3 complex. J.
862 Biol. Chem. 2008:**283**(11): 7135-7144.10.1074/jbc.M705894200
863 **Blanchoin L, and Staiger CJ.** Plant formins: Diverse isoforms and unique molecular mechanism.
864 Biochim. Biophys. Acta. 2010:**1803**(2): 201-206.10.1016/j.bbamcr.2008.09.015
865 **Blanchoin L, and Michelot A.** Actin cytoskeleton: a team effort during actin assembly. Curr. Biol.
866 2012:**22**(16): R643-R645.10.1016/j.cub.2012.07.026
867 **Burke TA, Christensen JR, Barone E, Suarez C, Sirotkin V, and Kovar DR.** Homeostatic actin
868 cytoskeleton networks are regulated by assembly factor competition for monomers.
869 Curr. Biol. 2014:**24**(5): 579-585.10.1016/j.cub.2014.01.072
870 **Cabrera R, Suo J, Young E, and Chang EC.** *Schizosaccharomyces pombe* Arc3 is a conserved
871 subunit of the Arp2/3 complex required for polarity, actin organization, and endocytosis.
872 Yeast. 2011:**28**(6): 495-503.10.1002/yea.1853
873 **Cai C, Henty-Ridilla JL, Szymanski DB, and Staiger CJ.** Arabidopsis myosin XI: a motor rules the
874 tracks. Plant Physiol. 2014:**166**(3): 1359-1370.10.1104/pp.114.244335
875 **Cao L, Henty-Ridilla JL, Blanchoin L, and Staiger CJ.** Profilin-dependent nucleation and assembly
876 of actin filaments controls cell elongation in Arabidopsis. Plant Physiol. 2016:**170**(1):
877 220-233.10.1104/pp.15.01321
878 **Carlier M-F, and Shekhar S.** Global treadmilling coordinates actin turnover and controls the size
879 of actin networks. Nat. Rev. Mol. Cell Biol. 2017:**18**(6): 389-401.10.1038/nrm.2016.172
880 **Chan FY, Silva AM, Saramago J, Pereira-Sousa J, Brighton HE, Pereira M, Oegema K, Gassmann**
881 **R, and Carvalho AX.** The ARP2/3 complex prevents excessive formin activity during
882 cytokinesis. Mol. Biol. Cell. 2019:**30**(1): 96-107.10.1091/mbc.E18-07-0471
883 **Chaudhry F, Guérin C, Von Witsch M, Blanchoin L, and Staiger CJ.** Identification
884 ofArabidopsisCyclase-associated Protein 1 as the First Nucleotide Exchange
885 Factor for Plant Actin. Mol. Biol. Cell. 2007:**18**(8): 3002-3014.10.1091/mbc.e06-11-1041

886 **Cheung AY, and Wu H-m.** Overexpression of an Arabidopsis formin stimulates supernumerary
887 actin cable formation from pollen tube cell membrane. Plant Cell. 2004:**16**(1): 257-
888 269.10.1105/tpc.016550
889 **Cifrová P, Oulehlová D, Kollárová E, Martinek J, Rosero A, Žárský V, Schwarzerová K, and**
890 **Cvrčková F.** Division of labor between two actin nucleators-the formin FH1 and the
891 ARP2/3 complex-in *Arabidopsis* epidermal cell morphogenesis. Front. Plant Sci.
892 2020:**11**(148.10.3389/fpls.2020.00148
893 **Courtemanche N, Pollard TD, and Chen Q.** Avoiding artefacts when counting polymerized actin
894 in live cells with LifeAct fused to fluorescent proteins. Nat. Cell Biol. 2016:**18**(6): 676-
895 683.10.1038/ncb3351
896 **Cui X, Zou M, and Li J.** Basally distributed actin array drives embryonic hypocotyl elongation
897 during the seed-to-seedling transition in Arabidopsis. New Phytol.
898 2023.10.1111/nph.19149
899 **Cvrčková F.** Formins and membranes: anchoring cortical actin to the cell wall and beyond.
900 Front. Plant Sci. 2013:**4**(436.10.3389/fpls.2013.00436
901 **Cvrčková F, Bavlnka B, and Žárský V.** Identification and cloning of AtFORMIN1, an *Arabidopsis*
902 *thaliana* formin homologue. Biochem. Soc. Trans. 2000:**28**(5): A208-
903 A208.10.1042/bst028a208c
904 **Cvrčková F, Novotný M, Pícková D, and Žárský V.** Formin homology 2 domains occur in
905 multiple contexts in angiosperms. BMC Genomics. 2004:**5**(1): 44.10.1186/1471-2164-5-
906 44
907 **Davidson AJ, Amato C, Thomason PA, and Insall RH.** WASP family proteins and formins
908 compete in pseudopod- and bleb-based migration. J. Cell Biol. 2018:**217**(2): 701-
909 714.10.1083/jcb.201705160
910 **Dayel MJ, and Mullins RD.** Activation of Arp2/3 complex: addition of the first subunit of the
911 new filament by a WASP protein triggers rapid ATP hydrolysis on Arp2. PLoS Biol.
912 2004:**2**(4): 476-485.10.1371/journal.pbio.0020091
913 **Deeks MJ, Hussey PJ, and Davies B.** Formins: intermediates in signal-transduction cascades that
914 affect cytoskeletal reorganization. Trends Plant Sci. 2002:**7**(11): 492-498.10.1016/s1360-
915 1385(02)02341-5
916 **Facette MR, Park Y, Sutimantanapi D, Luo A, Cartwright HN, Yang B, Bennett EJ, Sylvester AW,**
917 **and Smith LG.** The SCAR/WAVE complex polarizes PAN receptors and promotes division
918 asymmetry in maize. Nat. Plants. 2015:**1**(14024.10.1038/nplants.2014.24
919 **Flores LR, Keeling MC, Zhang X, Sliogeryte K, and Gavara N.** Lifeact-TagGFP2 alters F-actin
920 organization, cellular morphology and biophysical behaviour. Sci. Rep.
921 2019:**9**(1).10.1038/s41598-019-40092-w
922 **Fritzsche M, Erlenkamper C, Moeendarbary E, Charras G, and Kruse K.** Actin kinetics shapes
923 cortical network structure and mechanics. Sci Adv. 2016:**2**(4):
924 e1501337.10.1126/sciadv.1501337
925 **Fujiwara I, Suetsugu S, Uemura S, Takenawa T, and Ishiwata S.** Visualization and force
926 measurement of branching by Arp2/3 complex and N-WASP in actin filament. Biochem.
927 Biophys. Res. Commun. 2002:**293**(5): 1550-1555.10.1016/S0006-291X(02)00421-7

928 **Funk J, Merino F, Venkova L, Heydenreich L, Kierfeld J, Vargas P, Raunser S, Piel M, and**
929 **Bieling P.** Profilin and formin constitute a pacemaker system for robust actin filament
930 growth. eLife. 2019:**8**(10.7554/eLife.50963
931 **Gao X-Q, Wang X-L, Ren F, Chen J, and Wang X-C.** Dynamics of vacuoles and actin filaments in
932 guard cells and their roles in stomatal movement. Plant, Cell & Environment.
933 2009:**32**(8): 1108-1116.10.1111/j.1365-3040.2009.01993.x
934 **García-González J, Kebrlová Stpn, Semerák M, Lacek J, Kotannal Baby I, Petrášek J, and**
935 **Schwarzerová K.** Arp2/3 Complex Is Required for Auxin-Driven Cell Expansion Through
936 Regulation of Auxin Transporter Homeostasis. Front. Plant Sci.
937 2020:**11**(486.10.3389/fpls.2020.00486
938 **Hardham AR, Jones DA, and Takemoto D.** Cytoskeleton and cell wall function in penetration
939 resistance. Curr. Opin. Plant Biol. 2007:**10**(4): 342-348.10.1016/j.pbi.2007.05.001
940 **Harries PA, Pan A, and Quatrano RS.** Actin-related protein2/3 complex component ARPC1 is
941 required for proper cell morphogenesis and polarized cell growth in *Physcomitrella*
942 *patens*. Plant Cell. 2005:**17**(8): 2327-2339.10.1105/tpc.105.033266
943 **Henty JL, Bledsoe SW, Khurana P, Meagher RB, Day B, Blanchoin L, and Staiger CJ.** *Arabidopsis*
944 actin depolymerizing factor4 modulates the stochastic dynamic behavior of actin
945 filaments in the cortical array of epidermal cells. Plant Cell. 2011:**23**(10): 3711-
946 3726.10.1105/tpc.111.090670
947 **Henty-Ridilla JL, Li J, Blanchoin L, and Staiger CJ.** Actin dynamics in the cortical array of plant
948 cells. Curr. Opin. Plant Biol. 2013a:**16**(6): 678-687.10.1016/j.pbi.2013.10.012
949 **Henty-Ridilla JL, Shimono M, Li J, Chang JH, Day B, and Staiger CJ.** The plant actin cytoskeleton
950 responds to signals from microbe-associated molecular patterns. PLoS Pathog.
951 2013b:**9**(4): e1003290.10.1371/journal.ppat.1003290
952 **Hetrick B, Han MS, Helgeson LA, and Nolen BJ.** Small molecules CK-666 and CK-869 inhibit
953 actin-related protein 2/3 complex by blocking an activating conformational change.
954 Chem. Biol. 2013:**20**(5): 701-712.10.1016/j.chembiol.2013.03.019
955 **Higaki T, Akita K, and Katoh K.** Coefficient of variation as an image-intensity metric for
956 cytoskeleton bundling. Sci. Rep. 2020:**10**(1).10.1038/s41598-020-79136-x
957 **Higaki T, Kutsuna N, Sano T, Kondo N, and Hasezawa S.** Quantification and cluster analysis of
958 actin cytoskeletal structures in plant cells: role of actin bundling in stomatal movement
959 during diurnal cycles in Arabidopsis guard cells. Plant J. 2010:**61**(1): 156-
960 165.10.1111/j.1365-313x.2009.04032.x
961 **Hotulainen P, and Lappalainen P.** Stress fibers are generated by two distinct actin assembly
962 mechanisms in motile cells. the Journal of Cell Biology. 2006:**173**(3): 383-
963 394.10.1083/jcb.200511093
964 **Ichetovkin I, Grant W, and Condeelis J.** Cofilin produces newly polymerized actin filaments that
965 are preferred for dendritic nucleation by the Arp2/3 complex. Curr. Biol. 2002:**12**(1): 79-
966 84.10.1016/s0960-9822(01)00629-7
967 **Jiang K, Sorefan K, Deeks MJ, Bevan MW, Hussey PJ, and Hetherington AM.** The ARP2/3
968 complex mediates guard cell actin reorganization and stomatal movement in
969 *Arabidopsis*. Plant Cell. 2012:**24**(5): 2031-2040.10.1105/tpc.112.096263

970 **Kadzik RS, Homa KE, and Kovar DR.** F-actin cytoskeleton network self-organization through
971 competition and cooperation. Annu. Rev. Cell Dev. Biol. 2020:**36**(1): 35-
972 60.10.1146/annurev-cellbio-032320-094706
973 **Kovar DR.** Molecular details of formin-mediated actin assembly. Curr. Opin. Cell Biol.
974 2006:**18**(1): 11-17.10.1016/j.ceb.2005.12.011
975 **Kovar DR, and Pollard TD.** Progressing actin: Formin as a processive elongation machine. Nat.
976 Cell Biol. 2004:**6**(12): 1158-1159.10.1038/ncb1204-1158
977 **Kovar DR, Kuhn JR, Tichy AL, and Pollard TD.** The fission yeast cytokinesis formin Cdc12p is a
978 barbed end actin filament capping protein gated by profilin. J. Cell Biol. 2003:**161**(5):
979 875-887.10.1083/jcb.200211078
980 **Lan Y, Liu X, Fu Y, and Huang S.** *Arabidopsis* class I formins control membrane-originated actin
981 polymerization at pollen tube tips. PLOS Genet. 2018:**14**(11):
982 e1007789.10.1371/journal.pgen.1007789
983 **Le J, El-Assal SE-D, Basu D, Saad ME, and Szymanski DB.** Requirements for *Arabidopsis* ATARP2
984 and ATARP3 during Epidermal Development. Curr. Biol. 2003:**13**(15): 1341-
985 1347.10.1016/s0960-9822(03)00493-7
986 **Li J, and Staiger CJ.** Understanding Cytoskeletal Dynamics During the Plant Immune Response.
987 Annu Rev Phytopathol. 2018:**56**(513-533.10.1146/annurev-phyto-080516-035632
988 **Li J, Henty-Ridilla JL, Huang S, Wang X, Blanchoin L, and Staiger CJ.** Capping protein modulates
989 the dynamic behavior of actin filaments in response to phosphatidic acid in *Arabidopsis*.
990 Plant Cell. 2012:**24**(9): 3742-3754.10.1105/tpc.112.103945
991 **Li S, Blanchoin L, Yang Z, and Lord EM.** The putative Arabidopsis Arp2/3 complex controls leaf
992 cell morphogenesis. Plant Physiol. 2003:**132**(4): 2034-2044.10.1104/pp.103.028563
993 **Li X, Li J-H, Wang W, Chen N-Z, Ma T-S, Xi Y-N, Zhang X-L, Lin H-F, Bai Y, Huang S-J, and Chen Y-**
994 **L.** ARP2/3 complex-mediated actin dynamics is required for hydrogen peroxide-induced
995 stomatal closure in Arabidopsis. Plant Cell Environ. 2014:**37**(7): 1548-
996 1560.10.1111/pce.12259
997 **Liu H-K, Li Y-J, Wang S-J, Yuan T-L, Huang W-J, Dong X, Pei J-Q, Zhang D, McCormick S, and**
998 **Tang W-H.** Kinase partner protein plays a key role in controlling the speed and shape of
999 pollen tube growth in tomato. Plant Physiol. 2020:**184**(4): 1853-
1000 1869.10.1104/pp.20.01081
1001 **Lomakin AJ, Lee K-C, Han SJ, Bui DA, Davidson M, Mogilner A, and Danuser G.** Competition for
1002 actin between two distinct F-actin networks defines a bistable switch for cell
1003 polarization. Nat. Cell Biol. 2015:**17**(11): 1435-1445.10.1038/ncb3246
1004 **Mathur J, Mathur N, Kernebeck B, and Hulskamp M.** Mutations in actin-related proteins 2 and
1005 3 affect cell shape development in Arabidopsis. Plant Cell. 2003a:**15**(7): 1632-
1006 1645.10.1105/tpc.011676
1007 **Mathur J, Mathur N, Kirik V, Kernebeck B, Srinivas BP, and Hulskamp M.** *Arabidopsis*
1008 CROOKED encodes for the smallest subunit of the ARP2/3 complex and controls cell
1009 shape by region specific fine F-actin formation. Development. 2003b:**130**(14): 3137-
1010 3146.10.1242/dev.00549
1011 **Michelot A, Grassart A, Okreglak V, Costanzo M, Boone C, and Drubin DG.** Actin Filament
1012 Elongation in Arp2/3-Derived Networks Is Controlled by Three Distinct Mechanisms.
1013 Dev. Cell. 2013:**24**(2): 182-195.10.1016/j.devcel.2012.12.008

1014 **Michelot A, Berro J, Guérin C, Boujemaa-Paterski R, Staiger CJ, Martiel J-L, and Blanchoin L.**
1015 Actin-Filament Stochastic Dynamics Mediated by ADF/Cofilin. Curr. Biol. 2007:**17**(10):
1016 825-833.10.1016/j.cub.2007.04.037
1017 **Michelot A, Derivery E, Paterski-Boujemaa R, Guerin C, Huang S, Parcy F, Staiger CJ, and**
1018 **Blanchoin L.** A novel mechanism for the formation of actin-filament bundles by a
1019 nonprocessive formin. Curr. Biol. 2006:**16**(19): 1924-1930.10.1016/j.cub.2006.07.054
1020 **Michelot Ae, Guérin C, Huang S, Ingouff M, Richard Sp, Rodiuc N, Staiger CJ, and Blanchoin L.**
1021 The formin homology 1 domain modulates the actin nucleation and bundling activity of
1022 Arabidopsis FORMIN1. Plant Cell. 2005:**17**(8): 2296-2313.10.1105/tpc.105.030908
1023 **Mullins RD, Heuser JA, and Pollard TD.** The interaction of Arp2/3 complex with actin:
1024 Nucleation, high affinity pointed end capping, and formation of branching networks of
1025 filaments. Proc. Natl. Acad. Sci. USA. 1998:**95**(11): 6181-6186.10.1073/pnas.95.11.6181
1026 **Nishimura Y, Shi S, Li Q, Bershadsky AD, and Viasnoff V.** Crosstalk between myosin II and
1027 formin functions in the regulation of force generation and actomyosin dynamics in
1028 stress fibers. Cells Dev. 2021:**168**(203736.10.1016/j.cdev.2021.203736
1029 **Nolen BJ, Tomasevic N, Russell A, Pierce DW, Jia Z, McCormick CD, Hartman J, Sakowicz R, and**
1030 **Pollard TD.** Characterization of two classes of small molecule inhibitors of Arp2/3
1031 complex. Nature. 2009:**460**(7258): 1031-1034.10.1038/nature08231
1032 **Orman M, Landis M, Oza A, Nambiar D, Gjeci J, Song K, Huang V, Klestzick A, Hachicho C, Liu**
1033 **SQ, Kamm JM, Bartolini F, Vadakkan JJ, Rojas CM, and Vizcarra CL.** Alterations to the
1034 broad-spectrum formin inhibitor SMIFH2 improve potency (Cold Spring Harbor
1035 Laboratory),2022.
1036 **Paul AS, and Pollard TD.** The role of the FH1 domain and profilin in formin-mediated actin-
1037 filament elongation and nucleation. Curr. Biol. 2008:**18**(1): 9-
1038 19.10.1016/j.cub.2007.11.062
1039 **Peng X, Yan T, and Sun M.** The WASP-Arp2/3 complex signal cascade is involved in actin-
1040 dependent sperm nuclei migration during double fertilization in tobacco and maize. Sci.
1041 Rep. 2017:**7**(43161.10.1038/srep43161
1042 **Peremyslov VV, Cole RA, Fowler JE, and Dolja VV.** Myosin-Powered Membrane Compartment
1043 Drives Cytoplasmic Streaming, Cell Expansion and Plant Development. PLoS One.
1044 2015:**10**(10): e0139331.10.1371/journal.pone.0139331
1045 **Pollard TD.** Regulation of actin filament assembly by Arp2/3 complex and formins. Annu. Rev.
1046 Biophys. Biomol. Struct. 2007:**36**(451-477.10.1146/annurev.biophys.35.040405.101936
1047 **Pollard TD, Blanchoin L, and Mullins RD.** Molecular mechanisms controlling actin filament
1048 dynamics in nonmuscle cells. Annu. Rev. Biophys. Biomol. Struct. 2000:**29**(545-
1049 576.10.1146/annurev.biophys.29.1.545
1050 **Qi J, and Greb T.** Cell polarity in plants: the Yin and Yang of cellular functions. Curr. Opin. Plant
1051 Biol. 2017:**35**(105-110.10.1016/j.pbi.2016.11.015
1052 **Qiao Z, Sun H, Ng JTY, Ma Q, Koh SH, Mu Y, Miao Y, and Gao Y-G.** Structural and
1053 computational examination of the Arabidopsis profilin–Poly-P complex reveals
1054 mechanistic details in profilin-regulated actin assembly. Journal of Biological Chemistry.
1055 2019:**294**(49): 18650-18661.10.1074/jbc.ra119.011307
1056 **Qin L, Liu L, Tu J, Yang G, Wang S, Quilichini TD, Gao P, Wang H, Peng G, Blancaflor EB, Datla**
1057 **R, Xiang D, Wilson KE, and Wei Y.** The ARP2/3 complex, acting cooperatively with Class I

1058 formins, modulates penetration resistance in Arabidopsis against powdery mildew
1059 invasion. Plant Cell. 2021:**33**(9): 3151-3175.10.1093/plcell/koab170
1060 **Roh-Johnson M, and Goldstein B.** In vivo roles for Arp2/3 in cortical actin organization during *C.*
1061 *elegans* gastrulation. J. Cell Sci. 2009:**122**(21): 3983-3993.10.1242/jcs.057562
1062 **Romero S, Le Clainche C, Didry D, Egile C, Pantaloni D, and Carlier M-F.** Formin is a processive
1063 motor that requires profilin to accelerate actin assembly and associated ATP hydrolysis.
1064 Cell. 2004:**119**(3): 419-429.10.1016/j.cell.2004.09.039
1065 **Rosenbloom AD, Kovar EW, Kovar DR, Loew LM, and Pollard TD.** Mechanism of actin filament
1066 nucleation. Biophysical Journal 2021:**120**(20): 4399-4417.10.1016/j.bpj.2021.09.006
1067 **Rosero A, Žárský V, and Cvrčková F.** AtFH1 formin mutation affects actin filament and
1068 microtubule dynamics in *Arabidopsis thaliana*. J. Exp. Bot. 2013:**64**(2): 585-
1069 597.10.1093/jxb/ers351
1070 **Rosero A, Oulehlová D, Stillerová L, Schiebertová P, Grunt M, Žárský V, and Cvrčková F.**
1071 Arabidopsis FH1 formin affects cotyledon pavement cell shape by modulating
1072 cytoskeleton dynamics. Plant Cell Physiol. 2016:**57**(3): 488-504.10.1093/pcp/pcv209
1073 **Rouiller I, Xu X-P, Amann KJ, Egile C, Nickell S, Nicastro D, Li R, Pollard TD, Volkmann N, and**
1074 **Hanein D.** The structural basis of actin filament branching by the Arp2/3 complex. The
1075 Journal of Cell Biology. 2008:**180**(5): 887-895.10.1083/jcb.200709092
1076 **Sahi VP, Cifrová P, García-González J, Kotannal Baby I, Mouillé G, Gineau E, Müller K, Baluška**
1077 **Fe, Soukup A, Petrášek J, and Schwarzerová Ki.** *Arabidopsis thaliana* plants lacking the
1078 ARP2/3 complex show defects in cell wall assembly and auxin distribution. Ann. Bot.
1079 2018:**122**(5): 777-789.10.1093/aob/mcx178
1080 **Sampathkumar A, Gutierrez R, McFarlane HE, Bringmann M, Lindeboom J, Emons AM,**
1081 **Samuels L, Ketelaar T, Ehrhardt DW, and Persson S.** Patterning and lifetime of plasma
1082 membrane-localized cellulose synthase is dependent on actin organization in
1083 Arabidopsis interphase cells. Plant Physiol. 2013:**162**(2): 675-
1084 688.10.1104/pp.113.215277
1085 **Scheuring D, Lofke C, Kruger F, Kittelmann M, Eisa A, Hughes L, Smith RS, Hawes C,**
1086 **Schumacher K, and Kleine-Vehn J.** Actin-dependent vacuolar occupancy of the cell
1087 determines auxin-induced growth repression. Proc Natl Acad Sci U S A. 2016:**113**(2):
1088 452-457.10.1073/pnas.1517445113
1089 **Sept D, and McCammon JA.** Thermodynamics and kinetics of actin filament nucleation.
1090 Biophys. J. 2001:**81**(2): 667-674.10.1016/s0006-3495(01)75731-1
1091 **Sheahan MB, Staiger CJ, Rose RJ, and McCurdy DW.** A green fluorescent protein fusion to
1092 actin-binding domain 2 of Arabidopsis fimbrin highlights new features of a dynamic actin
1093 cytoskeleton in live plant cells. Plant Physiol. 2004:**136**(4): 3968-
1094 3978.10.1104/pp.104.049411
1095 **Spracklen AJ, Fagan TN, Lovander KE, and Tootle TL.** The pros and cons of common actin
1096 labeling tools for visualizing actin dynamics during Drosophila oogenesis. Dev Biol.
1097 2014:**393**(2): 209-226.10.1016/j.ydbio.2014.06.022
1098 **Staiger CJ, Poulter NS, Henty JL, Franklin-Tong VE, and Blanchoin L.** Regulation of actin
1099 dynamics by actin-binding proteins in pollen. J. Exp. Bot. 2010:**61**(7): 1969-
1100 1986.10.1093/jxb/erq012

1101 **Staiger CJ, Sheahan MB, Khurana P, Wang X, McCurdy DW, and Blanchoin L.** Actin filament
1102 dynamics are dominated by rapid growth and severing activity in the *Arabidopsis*
1103 cortical array. the Journal of Cell Biology. 2009:**184**(2): 269-280.10.1083/jcb.200806185
1104 **Suarez C, Carroll RT, Burke TA, Christensen JR, Bestul AJ, Sees JA, James ML, Sirotkin V, and**
1105 **Kovar DR.** Profilin regulates F-actin network homeostasis by favoring formin over
1106 Arp2/3 complex. Dev. Cell. 2015:**32**(1): 43-53.10.1016/j.devcel.2014.10.027
1107 **Sun H, Qiao Z, Chua KP, Tursic A, Liu X, Gao YG, Mu Y, Hou X, and Miao Y.** Profilin Negatively
1108 Regulates Formin-Mediated Actin Assembly to Modulate PAMP-Triggered Plant
1109 Immunity. Curr Biol. 2018:**28**(12): 1882-1895 e1887.10.1016/j.cub.2018.04.045
1110 **Sun S-C, Wang Q-L, Gao W-W, Xu Y-N, Liu H-L, Cui X-S, and Kim N-H.** Actin nucleator Arp2/3
1111 complex is essential for mouse preimplantation embryo development. Reprod. Fertil.
1112 Dev. 2013:**25**(4): 617-623.10.1071/RD12011
1113 **Szymanski DB, Marks MD, and Wick SM.** Organized F-actin is essential for normal trichome
1114 morphogenesis in Arabidopsis. Plant Cell. 1999:**11**(12): 2331-
1115 2347.10.1105/tpc.11.12.2331
1116 **Ueda H, Yokota E, Kutsuna N, Shimada T, Tamura K, Shimmen T, Hasezawa S, Dolja VV, and**
1117 **Hara-Nishimura I.** Myosin-dependent endoplasmic reticulum motility and F-actin
1118 organization in plant cells. Proc. Natl. Acad. Sci. USA. 2010:**107**(15): 6894-
1119 6899.10.1073/pnas.0911482107
1120 **van der Honing HS, van Bezouwen LS, Emons AM, and Ketelaar T.** High expression of Lifeact in
1121 Arabidopsis thaliana reduces dynamic reorganization of actin filaments but does not
1122 affect plant development. Cytoskeleton (Hoboken). 2011:**68**(10): 578-
1123 587.10.1002/cm.20534
1124 **van der Kammen R, Song J-Y, de Rink I, Janssen H, Madonna S, Scarponi C, Albanesi C,**
1125 **Brugman W, and Innocenti M.** Knockout of the Arp2/3 complex in epidermis causes a
1126 psoriasis-like disease hallmarked by hyperactivation of transcription factor Nrf2.
1127 Development. 2017:**144**(24): 4588-4603.10.1242/dev.156323
1128 **Vaškovičová K, Žárský V, Rösel D, Nikolič M, Buccione R, Cvrčková F, and Brábek J.** Invasive
1129 cells in animals and plants: searching for LECA machineries in later eukaryotic life. Biol.
1130 Direct. 2013:**8**(1): 8.10.1186/1745-6150-8-8
1131 **Vavylonis D, Kovar DR, O'Shaughnessy B, and Pollard TD.** Model of formin-associated actin
1132 filament elongation. Mol. Cell. 2006:**21**(4): 455-466.10.1016/j.molcel.2006.01.016
1133 **Vidali L, van Gisbergen PAC, Guerin C, Franco P, Li M, Burkart GM, Augustine RC, Blanchoin L,**
1134 **and Bezanilla M.** Rapid formin-mediated actin-filament elongation is essential for
1135 polarized plant cell growth. Proc. Natl. Acad. Sci. USA. 2009:**106**(32): 13341-
1136 13346.10.1073/pnas.0901170106
1137 **Wang P, Richardson C, Hawes C, and Hussey PJ.** *Arabidopsis* NAP1 Regulates the Formation of
1138 Autophagosomes. Curr. Biol. 2016:**26**(15): 2060-2069.10.1016/j.cub.2016.06.008
1139 **Wang P, Pleskot R, Zang J, Winkler J, Wang J, Yperman K, Zhang T, Wang K, Gong J, Guan Y,**
1140 **Richardson C, Duckney P, Vandorpe M, Mylle E, Fiserova J, Van Damme D, and Hussey**
1141 **PJ.** Plant AtEH/Pan1 proteins drive autophagosome formation at ER-PM contact sites
1142 with actin and endocytic machinery. Nat. Commun. 2019:**10**(1): 5132.10.1038/s41467-
1143 019-12782-6

1144 **Yanagisawa M, Zhang C, and Szymanski DB.** ARP2/3-dependent growth in the plant kingdom:
1145 SCARs for life. Front. Plant Sci. 2013:**4**(166.10.3389/fpls.2013.00166
1146 **Yanagisawa M, Alonso JM, and Szymanski DB.** Microtubule-dependent confinement of a cell
1147 signaling and actin polymerization control module regulates polarized cell growth. Curr.
1148 Biol. 2018:**28**(15): 2459-2466.e2454.10.1016/j.cub.2018.05.076
1149 **Yanagisawa M, Desyatova AS, Belteton SA, Mallery EL, Turner JA, and Szymanski DB.**
1150 Patterning mechanisms of cytoskeletal and cell wall systems during leaf trichome
1151 morphogenesis. Nat. Plants. 2015:**1**(15014.10.1038/nplants.2015.14
1152 **Zhang S, Liu C, Wang J, Ren Z, Staiger CJ, and Ren H.** A Processive *Arabidopsis* Formin
1153 Modulates Actin Filament Dynamics in Association with Profilin. Mol. Plant. 2016:**9**(6):
1154 900-910.10.1016/j.molp.2016.03.006
1155 **Zhang W, Cai C, and Staiger CJ.** Myosins XI are involved in exocytosis of cellulose synthase
1156 complexes. Plant Physiol. 2019:**179**(4): 1537-1555.10.1104/pp.19.00018
1157 **Zhang W, Huang L, Zhang C, and Staiger CJ.** Arabidopsis myosin XIK interacts with the exocyst
1158 complex to facilitate vesicle tethering during exocytosis. Plant Cell. 2021:**33**(7): 2454-
1159 2478.10.1093/plcell/koab116
1160

1161

1162 **Figure Legends**

1163 **Figure 1.** Genetic disruption of the Arp2/3 complex leads to reduced actin filament density and
1164 bundling.

1165 **A)** Representative images of epidermal cells from the apical region of 5-d-old etiolated
1166 hypocotyls expressing GFP-fABD2 imaged by variable angle epifluorescence microscopy
1167 (VAEM) are shown in left columns. Scale bar: 20 μm. Regions of interest (yellow boxes) were
1168 magnified and shown in right columns. Scale bar: 5 μm. **B–D)** Quantitative analysis of the
1169 percentage of occupancy or density of actin filament arrays **(B)** and the extent of filament
1170 bundling as measured by skewness **(C)** and coefficient of variance **(D)** analyses. Both the
1171 density and the bundling of actin arrays in *arp2-1* and *arpc2* cells were significantly decreased
1172 compared to those in the respective wild-type cells. In box-and-whisker plots, boxes show the
1173 interquartile range (IQR) and the median, and whiskers show the maximum-minimum interval of
1174 three biological repeats with independent populations of plants. Individual biological repeats are
1175 represented with different shapes (n = 30 seedlings, 10 seedlings per biological repeat). Letters
1176 [a–b] denote groups that show statistically significant differences with other genotypes by one-
1177 way ANOVA with Tukey's post-hoc test ($P < 0.05$).

1178

1179 **Figure 2.** Actin filament nucleation frequency is decreased by chemical or genetic inhibition of
1180 the Arp2/3 complex.

1181 **A)** Representative time-lapse series showing three subclasses of actin filament origin identified
1182 in hypocotyl epidermal cells: Actin filaments initiated *de novo* in the cytoplasm (top), from the
1183 side of a pre-existing filament (middle), or from the end of a pre-existing filament (bottom row).
1184 Blue dots; pre-existing filament. Magenta dots; new growing filament. Green arrowheads;
1185 nucleation site. Scale bar: 5 μm. **B–E)** Quantitative analysis of actin filament nucleation
1186 frequency, both overall **(B)** and by subclass of origin **(C–E)**. Hypocotyls were treated with
1187 DMSO solution (0.05% DMSO) or 10 μM CK-666 for 5 min prior to imaging with VAEM. The
1188 overall nucleation frequency **(B)** for each genotype or treatment was defined as the total number
1189 of filament origins per filament per minute in a 400 μm^2 region of interest. Total nucleation
1190 frequency in DMSO-treated wild-type cells was significantly higher than DMSO-treated *arp2-1*,
1191 CK-666-treated wild-type, or CK-666-treated *arp2-1* cells. When filament origin events were
1192 categorized into *de novo* **(C)**, side **(D)**, and end populations **(E)**, only the side-branching

1193 nucleation events showed a significant reduction in *arp2-1* and CK-666-treated cells compared
1194 to DMSO-treated wild type. In box-and-whisker plots, boxes show the interquartile range (IQR)
1195 and the median, and whiskers show the maximum-minimum interval of two biological repeats
1196 with independent populations of plants. Individual biological repeats are represented with
1197 different shapes (n = 20 seedlings, 10 seedlings per biological repeat). Letters [a–c] denote
1198 groups that show statistically significant differences with other genotypes or treatments by two-
1199 way ANOVA with Tukey's post-hoc test (P < 0.05).

1200

1201 **Figure 3.** Actin filament dynamic properties are altered when the Arp2/3 complex is inhibited.

1202 **A)** A representative actin filament was tracked during the elongation phase (top) and another
1203 filament was fragmented into pieces during the severing phase (bottom). Magenta dots; growing
1204 actin filament. Green arrowhead; nucleation site. White asterisk; elongating filament end. Yellow
1205 arrows; severing events. Scale bar: 10 μm. **B)** Quantitative analysis of the population
1206 distribution and average elongation rate of actin filaments in hypocotyl epidermal cells.
1207 Hypocotyls were treated with 0.05% DMSO solution or 10 μM CK-666 for 5 min prior to imaging
1208 with VAEM. The elongation rate distribution of DMSO-treated wild type had a single peak at
1209 1.25 – 1.75 μm/s, whereas the Arp2/3-inhibited groups had three peaks at 0.75 – 1.25 μm/s, 2.0
1210 – 2.5 μm/s, and > 3 μm/s. n ≥ 100 single filaments from two individual biological repeats (for one
1211 biological repeat, 5 single filaments were counted in one hypocotyl from at least 10 hypocotyls
1212 per genotype or treatment). Letters [a–b] denote genotypes or treatments that show statistically
1213 significant differences with other groups by Chi-squared test, P < 0.05. **C–E)** The average
1214 maximum length of side-branching filaments in DMSO-treated wild-type cells was significantly
1215 shorter than that in DMSO-treated *arp2-1*, CK-666-treated wild-type, or CK-666-treated *arp2-1*
1216 cells; however, filaments that originated *de novo* or from pre-existing ends did not show any
1217 significant difference. **F–H)** The average maximum lifetime of side-branching filaments in
1218 DMSO-treated wild-type cells was significantly shorter than that in DMSO-treated *arp2-1*, CK-
1219 666-treated wild-type, or CK-666-treated *arp2-1* cells; however, filaments that originated *de*
1220 *novo* or from pre-existing ends did not show any significant difference. **I–K)**, The severing
1221 frequency did not show any significant difference between different genotypes or treatments.
1222 For box-and-whisker plots, boxes show the interquartile range (IQR) and the median, and
1223 whiskers show the maximum-minimum interval of two biological repeats with independent
1224 populations of plants. Individual biological repeats are represented with different shapes (n = 20

1225 seedlings, 10 seedlings per biological repeat). Letters [a–b] denote groups that show statistically
1226 significant differences with other genotypes or treatments by two-way ANOVA with Tukey's
1227 post-hoc test (P < 0.05).

1228

1229 **Figure 4.** A small molecule inhibitor of the Arp2/3 complex, CK-666, reduces actin filament
1230 density and bundling.

1231 **A)** Representative images of epidermal cells from the apical region of 5-d-old etiolated
1232 hypocotyls are shown in left columns. Scale bar: 20 μm. Regions of interest (yellow boxes) were
1233 magnified and displayed in right columns. Scale bar: 5 μm. Hypocotyls were treated with 0.05%
1234 DMSO solution or 10 μM CK-666 for 5 min prior to imaging with VAEM. Actin filament arrays in
1235 DMSO-treated *arp2-1*, CK-666-treated *ARP2*, and CK-666-treated *arp2-1* cells appeared to be
1236 less dense and less bundled compared to DMSO-treated wild-type cells. **B–D)** Quantitative
1237 analysis of the percentage of occupancy or density of actin filament arrays **(B)**, and the extent of
1238 filament bundling as measured by skewness **(C)** and coefficient of variation **(D)** analyses. Both
1239 the density and bundling of actin arrays in DMSO-treated *arp2-1*, CK-666-treated wild-type and
1240 CK-666-treated *arp2-1* cells were significantly decreased compared to DMSO-treated wild-type
1241 cells. In box-and-whisker plots, boxes show the interquartile range (IQR) and the median, and
1242 whiskers show the maximum-minimum interval of three biological repeats with independent
1243 populations of plants. Individual biological repeats are represented with different shapes (n = 30
1244 seedlings, 10 seedlings per biological repeat). Letters [a–b] denote groups that show statistically
1245 significant differences with other genotypes or treatments by two-way ANOVA with Tukey's
1246 post-hoc test (P < 0.05).

1247

1248 **Figure 5.** Actin filament density increases after treatment of *arp2-1* with the formin inhibitor
1249 SMIFH2.

1250 **A)** Representative images of epidermal cells from the apical region of 5-d-old etiolated
1251 hypocotyls are shown in the left column. Scale bar: 20 μm. Regions of interest (yellow boxes)
1252 were magnified and displayed in the right column. Scale bar: 5 μm. Hypocotyls were treated
1253 with 0.05% DMSO solution or 25 μM SMIFH2 for 5 min prior to imaging with VAEM. Actin
1254 filament arrays in DMSO-treated *arp2-1* and SMIFH2-treated wild-type cells appeared to be less

1255 dense and less bundled compared to DMSO-treated wild-type cells, but SMIFH2-treated *arp2-1*
1256 cells have a significantly increased actin abundance. **B–D)** Quantitative analysis of the
1257 percentage of occupancy or density of actin filament arrays **(B)**, and the extent of filament
1258 bundling as measured by skewness **(C)** and coefficient of variation **(D)** analyses. The density of
1259 actin arrays in DMSO-treated *arp2-1* and SMIFH2-treated wild-type cells was significantly
1260 decreased compared to DMSO-treated wild type; however, SMIFH2-treated *arp2-1* cells had
1261 significantly increased actin density compared to all other genotypes and treatments **(B)**. Actin
1262 arrays in *arp2-1* or SMIFH2-treated cells were significantly less bundled compared to DMSO-
1263 treated wild-type cells **(C–D)**. In box-and-whisker plots, boxes show the interquartile range (IQR)
1264 and the median, and whiskers show the maximum-minimum interval of three biological repeats
1265 with independent populations of plants. Individual biological repeats are represented with
1266 different shapes (n = 30 seedlings, 10 seedlings per biological repeat). Letters [a–d] denote
1267 groups that show statistically significant differences with other genotypes or treatments by two-
1268 way ANOVA with Tukey's post-hoc test ($P < 0.05$).

1269

1270 **Figure 6.** Overall and *de novo* filament nucleation increase when Arp2/3 and formin activity are
1271 simultaneously inhibited.

1272 **A and C–E)** Quantitative analysis of actin filament nucleation frequency, both overall **(A)** and by
1273 the subclass of origin **(C–E)**. The total nucleation frequency in DMSO-treated *arp2-1* and
1274 SMIFH2-treated wild-type cells was significantly reduced compared to DMSO-treated wild-type
1275 cells. However, the total nucleation frequency of SMIFH2-treated *arp2-1* cells was significantly
1276 higher than all other genotypes and treatments **(A)** and this correlated with increased *de novo*
1277 nucleation events **(C)**. In box-and-whisker plots, boxes show the interquartile range (IQR) and
1278 the median, and whiskers show the maximum-minimum interval of two biological repeats with
1279 independent populations of plants. Individual biological repeats are represented with different
1280 shapes (n = 20 seedlings, 10 seedlings per biological repeat). Letters [a–c] denote groups that
1281 show statistically significant differences with other genotypes or treatments (within the same
1282 filament nucleation subclass) by two-way ANOVA with Tukey's post-hoc test ($P < 0.05$). **B)**
1283 Analysis of the population distribution of actin filament elongation rates. The elongation rate
1284 distribution of DMSO-treated wild type had a single peak at 1.25 – 1.75 μm/s, the DMSO-treated
1285 *arp2-1* had three peaks at 0.75 – 1.0 μm/s, 2.0 – 2.5 μm/s and > 3 μm/s, the SMIFH2-treated
1286 wild-type had a peak at 1.0 – 1.75 μm/s, but SMIFH2-treated *arp2-1* had peaks at 1.0 – 1.25

1287 μm/s and 1.75 – 2.0 μm/s. n ≥ 100 single filaments from two individual biological repeats (for
1288 one biological repeat, 5 single filaments were counted in one hypocotyl from at least 10
1289 hypocotyls per genotype or treatment). Letters [a–d] denote genotypes or treatments that show
1290 statistically significant differences with other groups by Chi-squared test, $P < 0.05$. **F–H)**, The
1291 average maximum length of filaments that originated *de novo* or from side-branching events in
1292 SMIFH2-treated *arp2-1* was significantly shorter than that in other cells, but filaments that
1293 originated from pre-existing ends did not show a difference between any genotype or treatment.
1294 **I–K)**, The average maximum lifetime of side-branching filaments in DMSO-treated *arp2-1*,
1295 SMIFH2-treated *arp2-1* and SMIFH2-treated wild-type cells were all significantly longer than the
1296 ones from DMSO-treated wild-type cells; however, filaments that originated *de novo* did not
1297 show any significant difference, and filaments that elongated from pre-existing ends in DMSO-
1298 treated wild-type cells were slightly shorter than SMIFH2-treated cells. **L–N)**, The severing
1299 frequency did not show any significant difference between different genotypes or treatments. In
1300 box-and-whisker plots, boxes show the interquartile range (IQR) and the median, and whiskers
1301 show the maximum-minimum interval of two biological repeats with independent populations of
1302 plants. Individual biological repeats are represented with different shapes (n = 20 seedlings, 10
1303 seedlings per biological repeat). Letters [a–c] denote groups that show statistically significant
1304 differences with other genotypes or treatments (within the same filament nucleation subclass)
1305 by two-way ANOVA with Tukey's post-hoc test ($P < 0.05$).

1306

1307 **Figure 7.** Filament abundance, total nucleation events and *de novo* filament formation increase
1308 when the Arp2/3 complex and formin activity are simultaneously reduced with chemical
1309 inhibitors.

1310 **A)** Representative images of epidermal cells from the apical region of 5-d-old etiolated
1311 hypocotyls are shown in left columns. Scale bar: 20 μm. Regions of interest (yellow boxes) were
1312 magnified and displayed in right columns. Scale bar: 5 μm. Hypocotyls were treated with 0.05%
1313 DMSO solution, 10 μM CK-666, 25 μM SMIFH2 or both inhibitors for 5 min prior to imaging with
1314 VAEM. Actin filament arrays in CK-666-treated cells and SMIFH2-treated cells appeared to be
1315 less dense and less bundled compared to mock-treated cells. However, dual treatment
1316 markedly increased actin filament abundance. **B–D)** Quantitative analysis of actin filament
1317 density **(B)** and extent of bundling by skewness **(C)** and coefficient of variation **(D)** analyses.
1318 The density of actin arrays in CK-666-treated and SMIFH2-treated cells was decreased

1319 compared to mock-treated cells; however, dual-treated (DUO) cells had significantly increased
1320 actin density compared to all other treatments. Actin arrays in CK-666- or dual-treated cells
1321 were significantly less bundled than in mock-treated cells. In box-and-whisker plots, boxes show
1322 the interquartile range (IQR) and the median, and whiskers show the maximum-minimum
1323 interval of three biological repeats with independent populations of plants. Individual biological
1324 repeats are represented with different shapes (n = 30 seedlings, 10 seedlings per biological
1325 repeat). Letters [a–c] denote groups that show statistically significant differences with other
1326 genotypes or treatments by two-way ANOVA with Tukey's post-hoc test ($P < 0.05$). **E–H)**
1327 Quantitative analysis of actin filament nucleation frequency, both overall **(E)** and by subclass of
1328 origin **(F– H)**. The total nucleation frequency in mock-treated cells was higher than CK-666-
1329 treated and SMIFH2-treated cells. However, the total nucleation frequency of dual-treated
1330 (DUO) cells was significantly higher than all other treatments and this correlated with increased
1331 *de novo* nucleation events. In box-and-whisker plots, boxes show the interquartile range (IQR)
1332 and the median, and whiskers show the maximum-minimum interval of two biological repeats
1333 with independent populations of plants. Individual biological repeats are represented with
1334 different shapes (n = 20 seedlings, 10 seedlings per biological repeat). Letters [a–c] denote
1335 groups that show statistically significant differences with other genotypes or treatments by two-
1336 way ANOVA with Tukey's post-hoc test ($P < 0.05$).

1337

1338 **Figure 8.** SMIFH2 treatment results in further reduction of both actin density and actin filament
1339 nucleation frequency in the *fh1-2* mutant.

1340 **A)** Representative images of epidermal cells from the apical region of 5-d-old etiolated
1341 hypocotyls are shown in the left columns. Scale bar: 20 μm. Regions of interest (yellow boxes)
1342 were magnified and displayed in the right columns. Scale bar: 5 μm. Hypocotyls were treated
1343 with 0.05% DMSO solution, 10 μM CK-666, 25 μM SMIFH2 or both inhibitors for 5 min prior to
1344 imaging. Actin filament arrays in either DMSO-treated or single-inhibitor-treated *fh1-2* cells all
1345 appeared to be less dense compared to DMSO-treated wild-type cells, but both dual-inhibitor-
1346 treated wild-type and *fh1-2* cells appeared to have more dense actin arrays compared to
1347 DMSO-treated wild-type cells. **B–D)** Quantitative analysis of the percentage of occupancy or
1348 density of actin filament arrays **(B)** and the extent of filament bundling as measured by
1349 skewness **(C)** and coefficient of variance **(D)** analyses. The density of actin arrays in DMSO-
1350 treated *fh1-2* cells was significantly decreased but the extent of filament bundling was increased

1351 compared to DMSO-treated wild-type cells. Treatment with either CK-666 or SMIFH2 caused an
1352 additional decrease in actin density in *fh1-2* cells and filaments were less bundled compared to
1353 DMSO-treated wild-type. However, simultaneous treatment with both inhibitors (DUO)
1354 significantly increased actin array density in both wild-type and *fh1-2* cells. In box-and-whisker
1355 plots, boxes show the interquartile range (IQR) and the median, and whiskers show the
1356 maximum-minimum interval of two biological repeats with independent populations of plants.
1357 Individual biological repeats are represented with different shapes (n = 20 seedlings, 10
1358 seedlings per biological repeat). Letters [a–d] denote groups that show statistically significant
1359 differences with other genotypes or treatments by two-way ANOVA with Tukey's post-hoc test
1360 ($P < 0.05$). **E–H)** Quantitative analysis of actin filament nucleation frequency, both overall **(E)**
1361 and by subclass of origin **(F–H)**. The total nucleation frequency in DMSO-treated *fh1-2* cells was
1362 significantly reduced compared to DMSO-treated wild-type cells, and either CK-666 or SMIFH2
1363 treatment caused an additional decrease in overall filament nucleation in *fh1-2* cells **(E)**.
1364 However, the total nucleation frequency of dual-inhibitor-treated *fh1-2* or wild-type cells was
1365 significantly higher than all other genotypes and treatments **(E)** and this correlated with
1366 increased *de novo* nucleation events **(F)**. In box-and-whisker plots, boxes show the interquartile
1367 range (IQR) and the median, and whiskers show the maximum-minimum interval of two
1368 biological repeats with independent populations of plants. Individual biological repeats are
1369 represented with different shapes (n = 20 seedlings, 10 seedlings per biological repeat). Letters
1370 [a–d] denote groups that show statistically significant differences with other genotypes or
1371 treatments by two-way ANOVA with Tukey's post-hoc test ($P < 0.05$).

1372

1373 **Figure 9.** Increased filament abundance, total nucleation events and *de novo* filament formation
1374 following simultaneous CK-666 and SMIFH2 treatment are further enhanced in the *prf1-2*
1375 mutant.

1376 **A)** Representative images of epidermal cells from the apical region of 5-d-old etiolated
1377 hypocotyls are shown in the left columns. Scale bar: 20 μm. Regions of interest (yellow boxes)
1378 were magnified and displayed in the right columns. Scale bar: 5 μm. Hypocotyls were treated
1379 with 0.05% DMSO solution, 10 μM CK-666, 25 μM SMIFH2 or both inhibitors for 5 min prior to
1380 imaging with VAEM. Actin filament arrays in either DMSO-treated or single-inhibitor-treated *prf1-*
1381 *2* cells all appeared to be less dense and less bundled compared to DMSO-treated wild-type
1382 cells, but both dual-inhibitor-treated wild-type and *prf1-2* cells appeared to have more dense

1383 actin arrays compared to DMSO-treated wild-type cells. **B–D)** Quantitative analysis of actin
1384 filament density **(B)** and extent of bundling by skewness **(C)** and coefficient of variation **(D)**
1385 analyses. The density of actin arrays in either DMSO-treated or single-inhibitor-treated *prf1-2*
1386 cells was significantly decreased compared to DMSO-treated wild-type cells; however, the
1387 treatment with both inhibitors (DUO) significantly increased the actin density in both wild-type
1388 and *prf1-2* cells. Actin arrays were less bundled when either Arp2/3, formins or PRF1 were
1389 inhibited compared to DMSO-wild-type cells. In box-and-whisker plots, boxes show the
1390 interquartile range (IQR) and the median, and whiskers show the maximum-minimum interval of
1391 three biological repeats with independent populations of plants. Individual biological repeats are
1392 represented with different shapes (n = 30 seedlings, 10 seedlings per biological repeat). Letters
1393 [a–f] denote groups that show statistically significant differences with other genotypes or
1394 treatments by two-way ANOVA with Tukey's post-hoc test ($P < 0.05$). **E–H)** Quantitative
1395 analysis of actin filament nucleation frequency, both overall **(E)** and by subclass of origin **(F–H)**.
1396 The total nucleation frequency in DMSO-treated, CK-666-treated and SMIFH2-treated *prf1-2*
1397 cells was significantly reduced compared to DMSO-treated wild-type cells. However, the total
1398 nucleation frequency of dual-inhibitor-treated (DUO) *prf1-2* **(E)** was significantly higher than all
1399 other genotypes and treatments and this corresponded to a significant increase in *de novo*
1400 nucleation events **(F)**. In box-and-whisker plots, boxes show the interquartile range (IQR) and
1401 the median, and whiskers show the maximum-minimum interval of two biological repeats with
1402 independent populations of plants. Individual biological repeats are represented with different
1403 shapes (n = 20 seedlings, 10 seedlings per biological repeat). Letters [a–e] denote groups that
1404 show statistically significant differences with other genotypes or treatments by two-way ANOVA
1405 with Tukey's post-hoc test ($P < 0.05$).

1406

Figures & Figure Legends

Table 1. Single actin filament dynamics in wild type (*ARP2*) and *arp2-1* mutant with or without CK-666.

Stochastic Dynamic Parameters	Genotype & Treatment			
	ARP2 w/ DMSO	*arp2-1* w/ DMSO	*ARP2* w/ CK-666	*arp2-1* w/ CK-666
Elongation Rate; µm/s	1.79 ± 0.05 [a]	1.90 ± 0.07 [b]	1.89 ± 0.07 [b]	1.90 ± 0.07 [b]
Max. Filament Length; µm	16.6 ± 0.3 [a]	17.4 ± 0.2 [b]	17.2 ± 0.2 [b]	17.8 ± 0.3 [b]
Max. Filament Lifetime; s	18.7 ± 0.4 [a]	22.6 ± 0.3 [b]	22.0 ± 0.3 [b]	22.9 ± 0.3 [b]
Severing Frequency; breaks/mm/s	8.20 ± 0.11 [a]	7.93 ± 0.12 [a]	7.60 ± 0.19 [b]	8.18 ± 0.20 [a]

Measurements were taken from epidermal cells in the elongating apical region of 5-d-old dark-grown hypocotyls. Values represent mean ± SE. n ≥ 100 filaments from two biological repeats conducted with independent plant materials (for one biological repeat, 5 filaments were counted in one hypocotyl from at least 10 hypocotyls per treatment/genotype). Two-way ANOVA with Tukey's post-hoc test, letters [a–b] denote genotypes or treatments that show statistically significant differences with other genotypes or treatments, $P < 0.05$

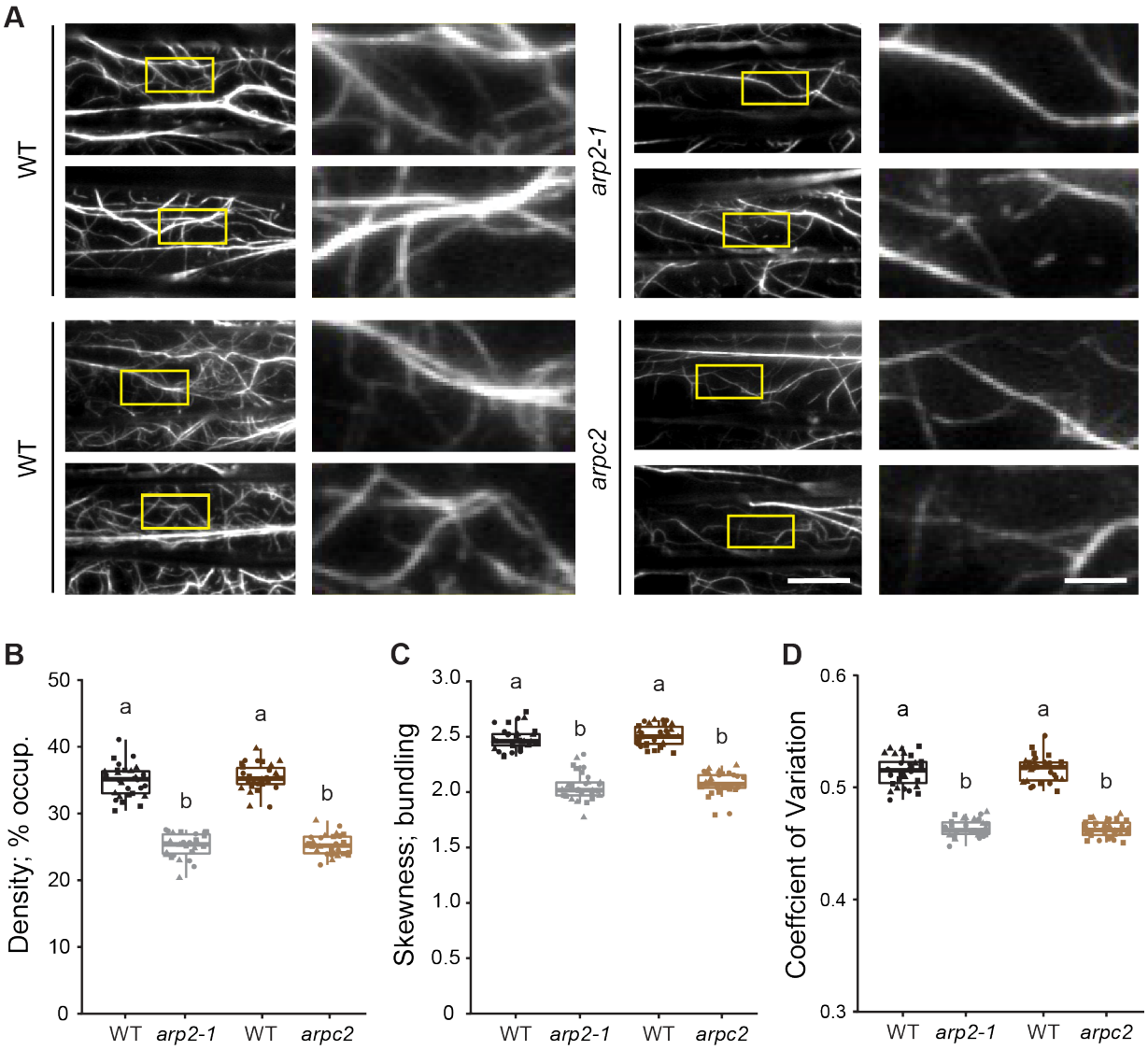

Figure 1. Genetic disruption of the Arp2/3 complex leads to reduced actin filament density and bundling.

A) Representative images of epidermal cells from the apical region of 5-d-old etiolated hypocotyls expressing GFP-fABD2 imaged by variable angle epifluorescence microscopy (VAEM) are shown in left columns. Scale bar: 20 µm. Regions of interest (yellow boxes) were magnified and shown in right columns. Scale bar: 5 µm. **B–D)** Quantitative analysis of the percentage of occupancy or density of actin filament arrays **(B)** and the extent of filament bundling as measured by skewness **(C)** and coefficient of variance **(D)** analyses. Both the density and the bundling of actin arrays in *arp2-1* and *arpc2* cells were significantly decreased compared to those in the respective wild-type cells. In box-and-whisker plots, boxes show the interquartile range (IQR) and the median, and whiskers show the maximum-minimum interval of three biological repeats with independent populations of plants. Individual biological repeats are represented with different shapes (n = 30 seedlings, 10 seedlings per biological repeat). Letters [a–b] denote groups that show statistically significant differences with other genotypes by one-way ANOVA with Tukey's post-hoc test ($P < 0.05$).

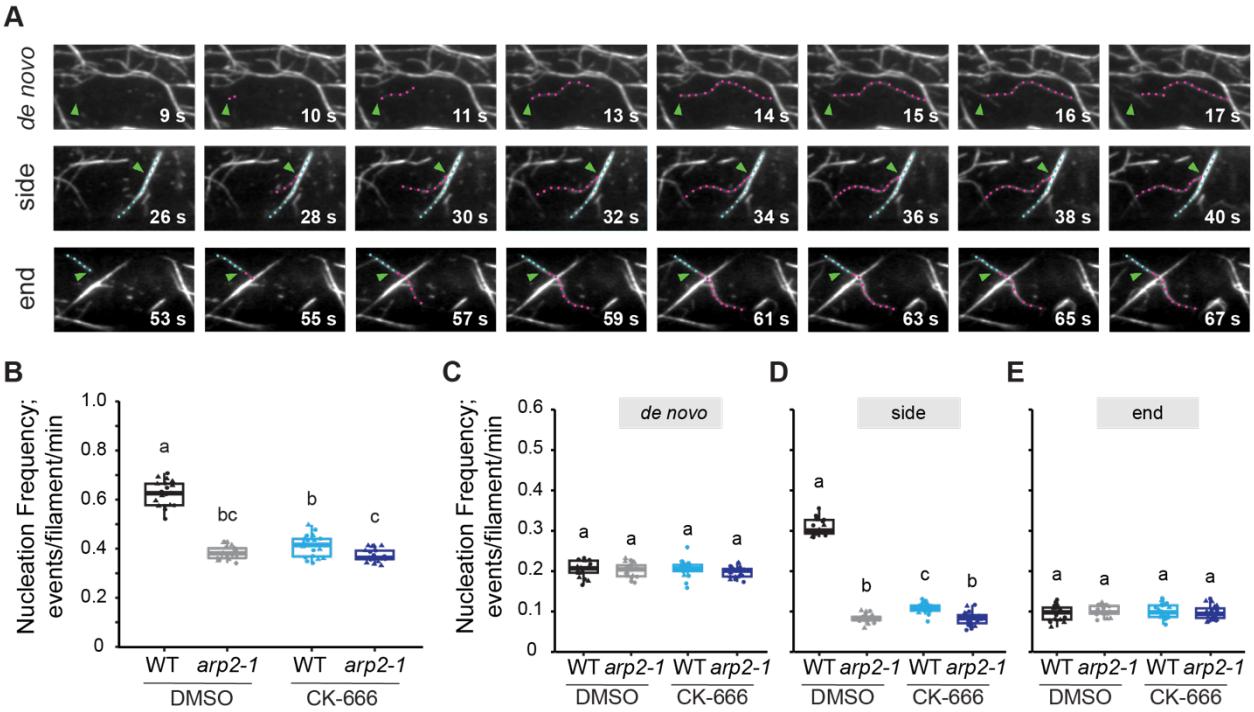

Figure 2. Actin filament nucleation frequency is decreased by chemical or genetic inhibition of the Arp2/3 complex.

A) Representative time-lapse series showing three subclasses of actin filament origin identified in hypocotyl epidermal cells: Actin filaments initiated *de novo* in the cytoplasm (top), from the side of a pre-existing filament (middle), or from the end of a pre-existing filament (bottom row). Blue dots; pre-existing filament. Magenta dots; new growing filament. Green arrowheads; nucleation site. Scale bar: 5 µm. **B–E)** Quantitative analysis of actin filament nucleation frequency, both overall **(B)** and by subclass of origin **(C–E)**. Hypocotyls were treated with DMSO solution (0.05% DMSO) or 10 µM CK-666 for 5 min prior to imaging with VAEM. The overall nucleation frequency **(B)** for each genotype or treatment was defined as the total number of filament origins per filament per minute in a 400 μm^2 region of interest. Total nucleation frequency in DMSO-treated wild-type cells was significantly higher than DMSO-treated *arp2-1*, CK-666-treated wild-type, or CK-666-treated *arp2-1* cells. When filament origin events were categorized into *de novo* **(C)**, side **(D)**, and end populations **(E)**, only the side-branching nucleation events showed a significant reduction in *arp2-1* and CK-666-treated cells compared to DMSO-treated wild type. In box-and-whisker plots, boxes show the interquartile range (IQR) and the median, and whiskers show the maximum-minimum interval of two biological repeats with independent populations of plants. Individual biological repeats are represented with different shapes (n = 20 seedlings, 10 seedlings per biological repeat). Letters [a–c] denote groups that show statistically significant differences with other genotypes or treatments by two-way ANOVA with Tukey's post-hoc test ($P < 0.05$).

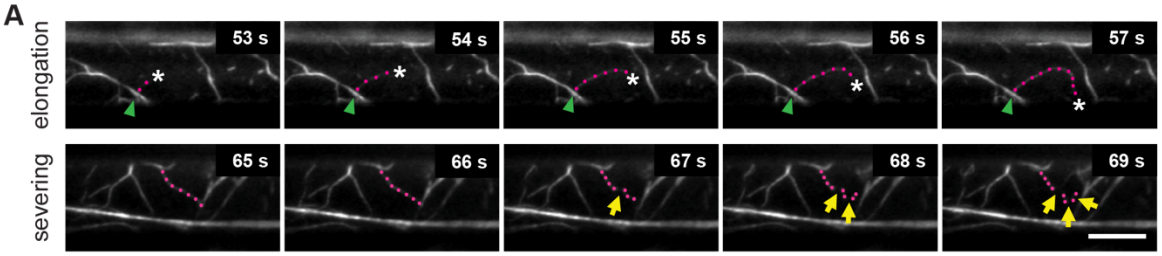
A
elongation
severing
53 s
54 s
55 s
56 s
57 s
65 s
66 s
67 s
68 s
69 s

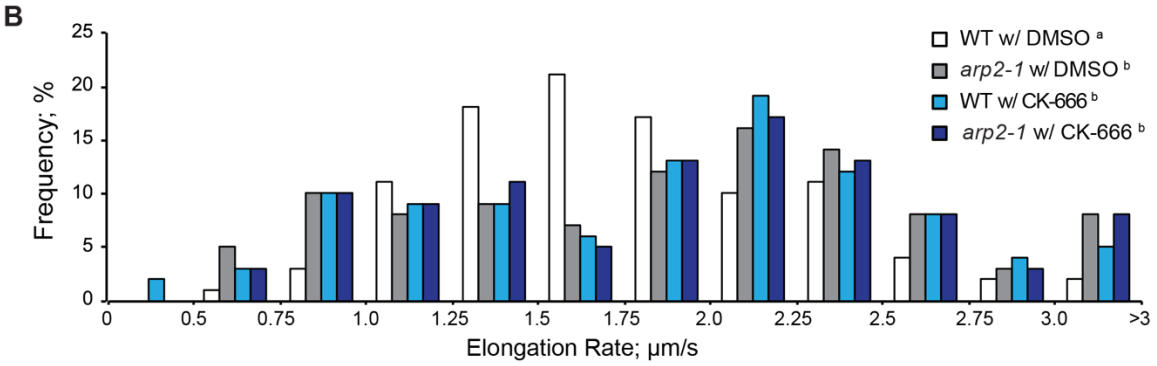
B
Frequency; %
Elongation Rate; µm/s
WT w/ DMSO a
arp2-1 w/ DMSO b
WT w/ CK-666 b
arp2-1 w/ CK-666 b

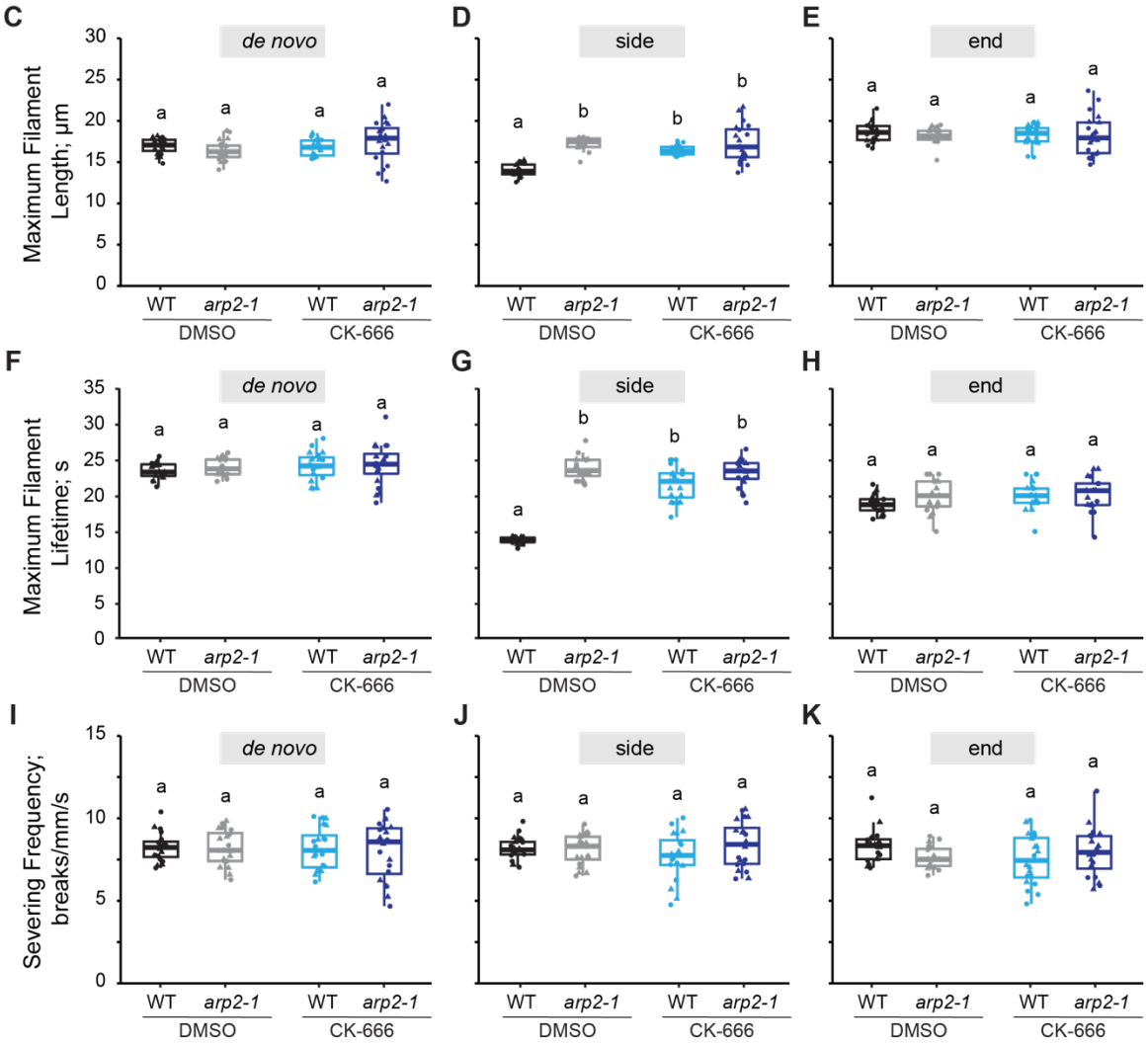
C
D
E
F
G
H
I
J
K
de novo
side
end
Maximum Filament Length; µm
Maximum Filament Lifetime; s
Severing Frequency; breaks/mm/s
WT
arp2-1
DMSO
CK-666

Figure 3. Actin filament dynamic properties are altered when the Arp2/3 complex is inhibited.

A) A representative actin filament was tracked during the elongation phase (top) and another filament was fragmented into pieces during the severing phase (bottom). Magenta dots; growing actin filament. Green arrowhead; nucleation site. White asterisk; elongating filament end. Yellow arrows; severing events. Scale bar: 10 μm. **B)** Quantitative analysis of the population distribution and average elongation rate of actin filaments in hypocotyl epidermal cells. Hypocotyls were treated with 0.05% DMSO solution or 10 μM CK-666 for 5 min prior to imaging with VAEM. The elongation rate distribution of DMSO-treated wild type had a single peak at 1.25 – 1.75 μm/s, whereas the Arp2/3-inhibited groups had three peaks at 0.75 – 1.25 μm/s, 2.0 – 2.5 μm/s, and > 3 μm/s. n ≥ 100 single filaments from two individual biological repeats (for one biological repeat, 5 single filaments were counted in one hypocotyl from at least 10 hypocotyls per genotype or treatment). Letters [a–b] denote genotypes or treatments that show statistically significant differences with other groups by Chi-squared test, $P < 0.05$. **C–E)** The average maximum length of side-branching filaments in DMSO-treated wild-type cells was significantly shorter than that in DMSO-treated *arp2-1*, CK-666-treated wild-type, or CK-666-treated *arp2-1* cells; however, filaments that originated *de novo* or from pre-existing ends did not show any significant difference. **F–H)** The average maximum lifetime of side-branching filaments in DMSO-treated wild-type cells was significantly shorter than that in DMSO-treated *arp2-1*, CK-666-treated wild-type, or CK-666-treated *arp2-1* cells; however, filaments that originated *de novo* or from pre-existing ends did not show any significant difference. **I–K)**, The severing frequency did not show any significant difference between different genotypes or treatments. For box-and-whisker plots, boxes show the interquartile range (IQR) and the median, and whiskers show the maximum-minimum interval of two biological repeats with independent populations of plants. Individual biological repeats are represented with different shapes (n = 20 seedlings, 10 seedlings per biological repeat). Letters [a–b] denote groups that show statistically significant differences with other genotypes or treatments by two-way ANOVA with Tukey's post-hoc test ($P < 0.05$).

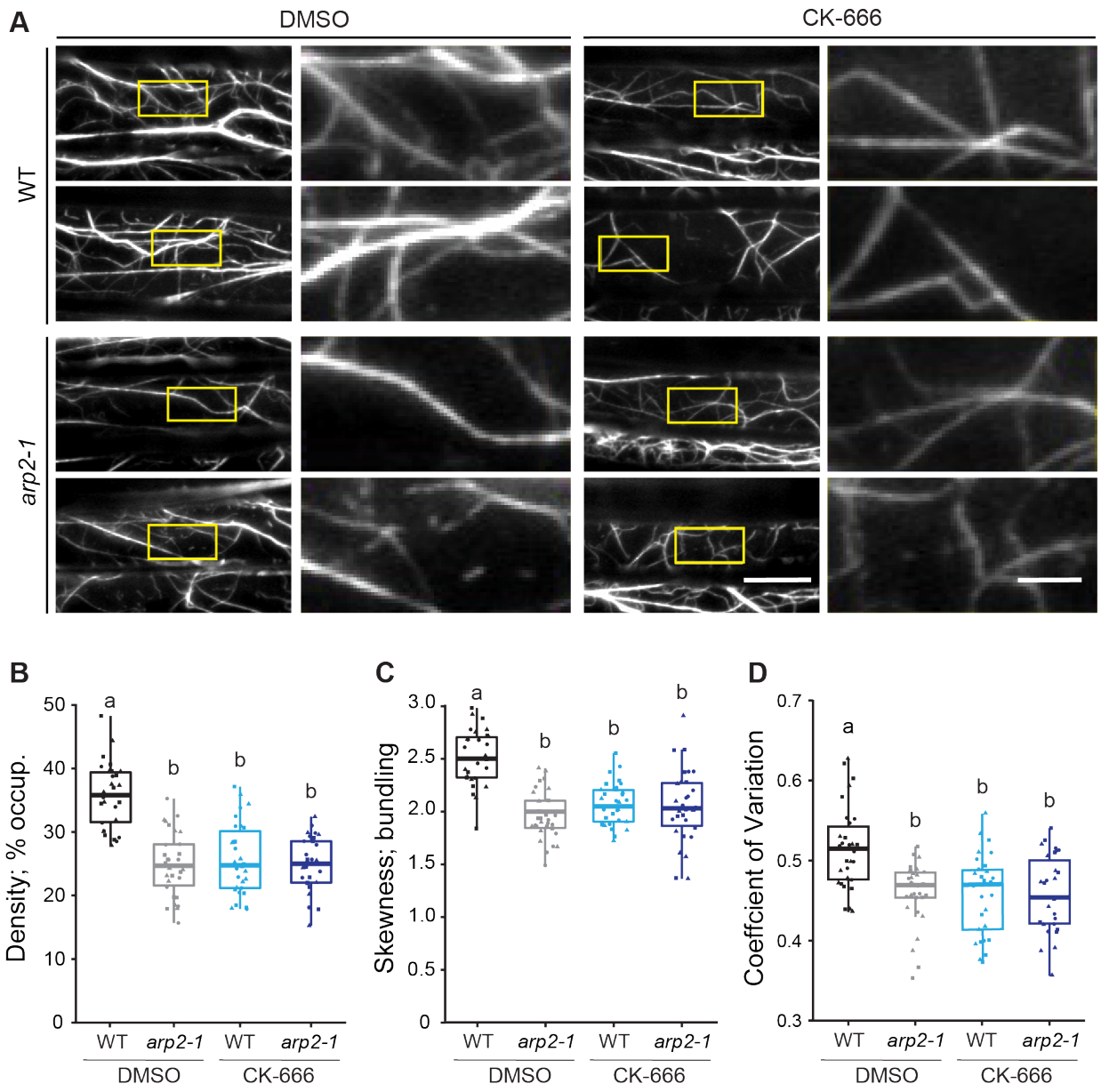

Figure 4. A small molecule inhibitor of the Arp2/3 complex, CK-666, reduces actin filament density and bundling.

A) Representative images of epidermal cells from the apical region of 5-d-old etiolated hypocotyls are shown in left columns. Scale bar: 20 µm. Regions of interest (yellow boxes) were magnified and displayed in right columns. Scale bar: 5 µm. Hypocotyls were treated with 0.05% DMSO solution or 10 µM CK-666 for 5 min prior to imaging with VAEM. Actin filament arrays in DMSO-treated *arp2-1*, CK-666-treated *ARP2*, and CK-666-treated *arp2-1* cells appeared to be less dense and less bundled compared to DMSO-treated wild-type cells. **B–D)** Quantitative analysis of the percentage of occupancy or density of actin filament arrays **(B)**, and the extent of filament bundling as measured by skewness **(C)** and coefficient of variation **(D)** analyses. Both the density and bundling of actin arrays in DMSO-treated *arp2-1*, CK-666-treated wild-type and CK-666-treated *arp2-1* cells were significantly decreased

compared to DMSO-treated wild-type cells. In box-and-whisker plots, boxes show the interquartile range (IQR) and the median, and whiskers show the maximum-minimum interval of three biological repeats with independent populations of plants. Individual biological repeats are represented with different shapes (n = 30 seedlings, 10 seedlings per biological repeat). Letters [a–b] denote groups that show statistically significant differences with other genotypes or treatments by two-way ANOVA with Tukey's post-hoc test ($P < 0.05$).

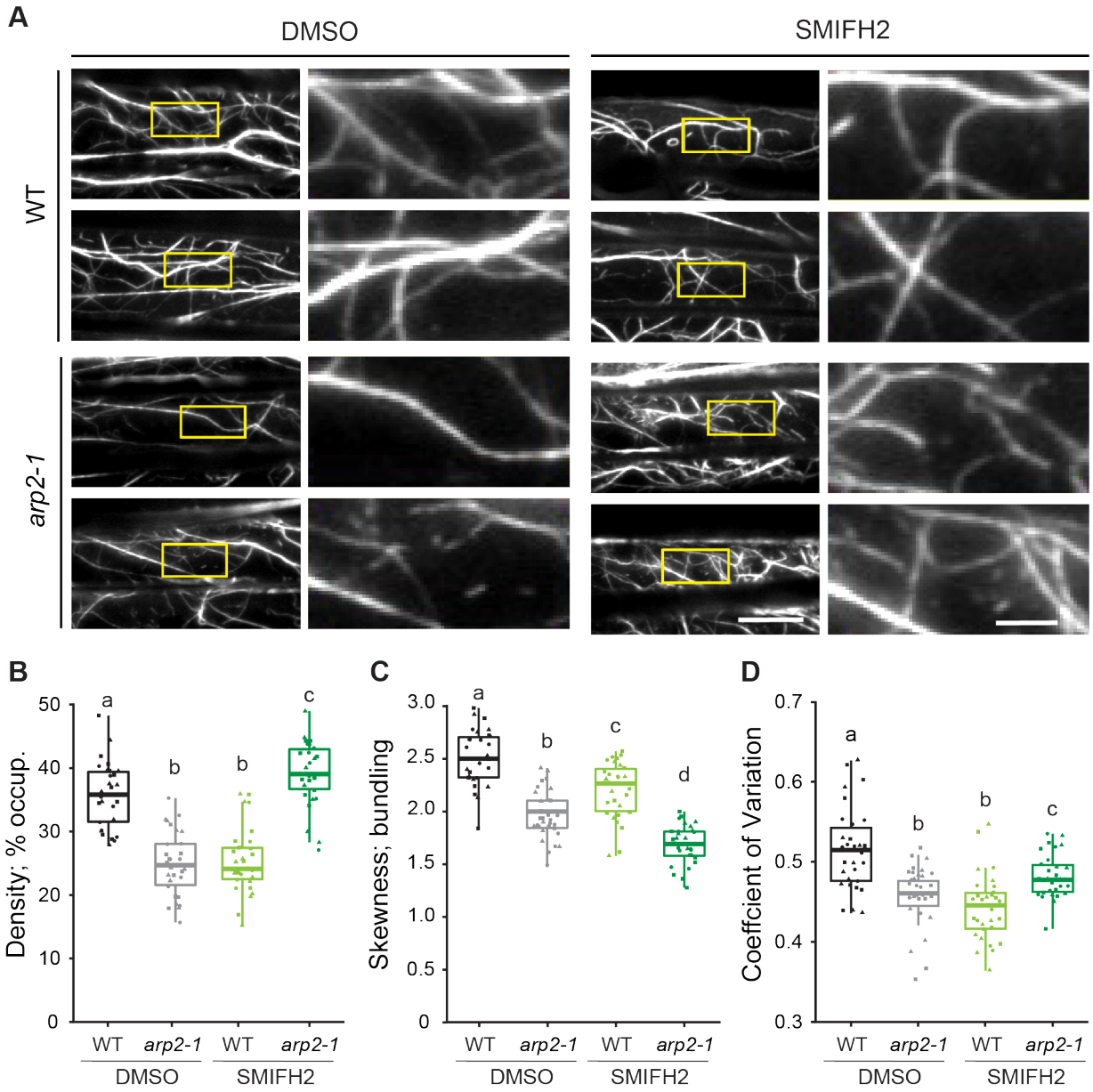

Figure 5. Actin filament density increases after treatment of *arp2-1* with the formin inhibitor SMIFH2.

A) Representative images of epidermal cells from the apical region of 5-d-old etiolated hypocotyls are shown in the left column. Scale bar: 20 µm. Regions of interest (yellow boxes) were magnified and displayed in the right column. Scale bar: 5 µm. Hypocotyls were treated with 0.05% DMSO solution or 25 µM SMIFH2 for 5 min prior to imaging with VAEM. Actin filament arrays in DMSO-treated *arp2-1* and SMIFH2-treated wild-type cells appeared to be less dense and less bundled compared to DMSO-treated wild-type cells, but SMIFH2-treated *arp2-1* cells have a significantly increased actin abundance. **B–D)** Quantitative analysis of the percentage of occupancy or density of actin filament arrays **(B)**, and the extent of filament bundling as measured by skewness **(C)** and coefficient of variation **(D)** analyses. The density of actin arrays in DMSO-treated *arp2-1* and SMIFH2-treated wild-type cells was significantly decreased compared to DMSO-treated wild type; however, SMIFH2-treated *arp2-1* cells had significantly

increased actin density compared to all other genotypes and treatments **(B)**. Actin arrays in *arp2-1* or SMIFH2-treated cells were significantly less bundled compared to DMSO-treated wild-type cells **(C–D)**. In box-and-whisker plots, boxes show the interquartile range (IQR) and the median, and whiskers show the maximum-minimum interval of three biological repeats with independent populations of plants. Individual biological repeats are represented with different shapes (n = 30 seedlings, 10 seedlings per biological repeat). Letters [a–d] denote groups that show statistically significant differences with other genotypes or treatments by two-way ANOVA with Tukey's post-hoc test ($P < 0.05$).

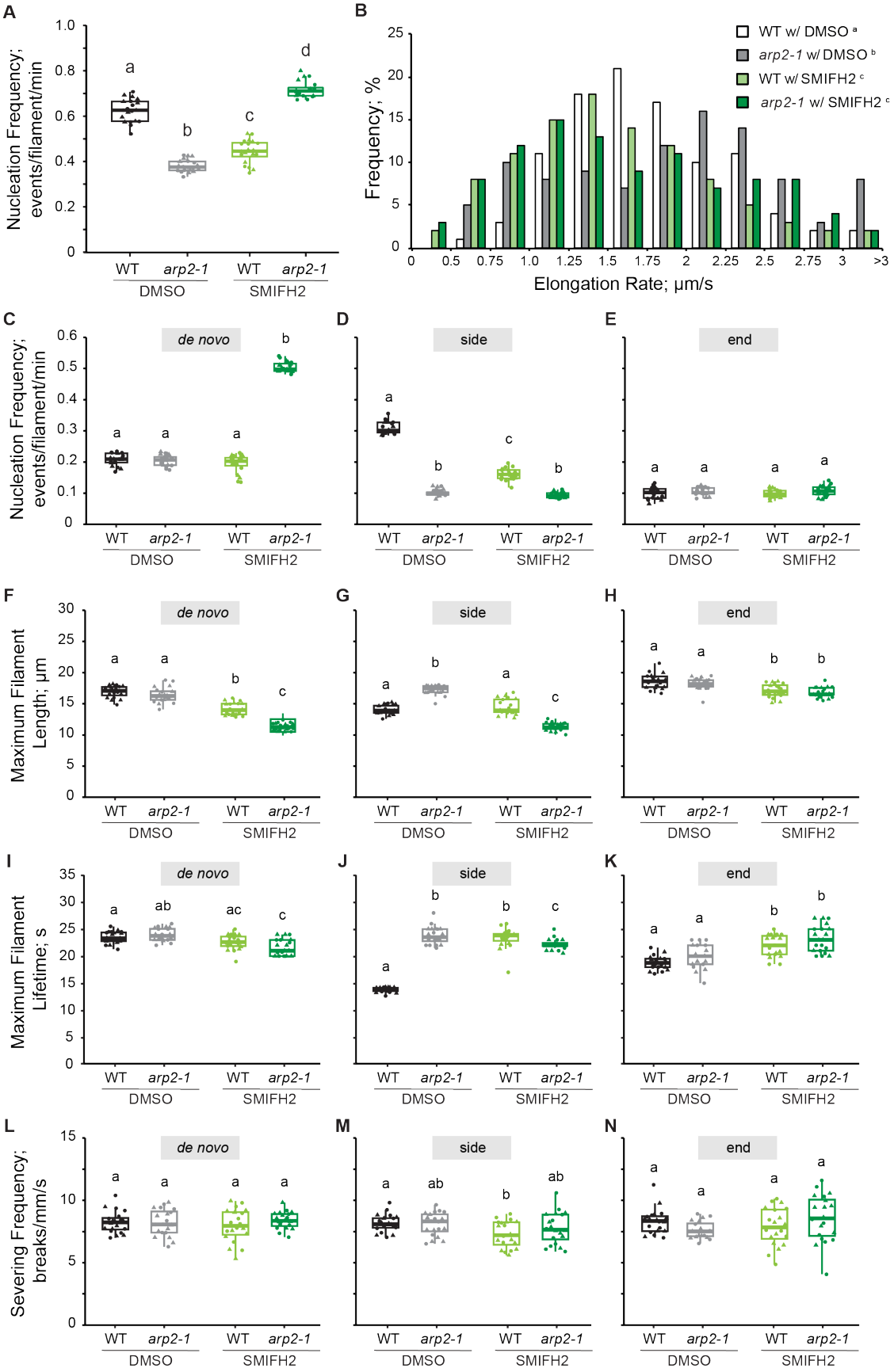
A
Nucleation Frequency; events/filament/min
WT
arp2-1
DMSO
SMIFH2
B
Frequency; %
Elongation Rate; µm/s
WT w/ DMSO a
arp2-1 w/ DMSO b
WT w/ SMIFH2 c
arp2-1 w/ SMIFH2 c
C
D
E
de novo
side
end
F
G
H
Maximum Filament Length; µm
I
J
K
Maximum Filament Lifetime; s
L
M
N
Severing Frequency; breaks/mm/s

Figure 6. Overall and *de novo* filament nucleation increase when Arp2/3 and formin activity are simultaneously inhibited.

A and C–E) Quantitative analysis of actin filament nucleation frequency, both overall **(A)** and by the subclass of origin **(C–E)**. The total nucleation frequency in DMSO-treated *arp2-1* and SMIFH2-treated wild-type cells was significantly reduced compared to DMSO-treated wild-type cells. However, the total nucleation frequency of SMIFH2-treated *arp2-1* cells was significantly higher than all other genotypes and treatments **(A)** and this correlated with increased *de novo* nucleation events **(C)**. In box-and-whisker plots, boxes show the interquartile range (IQR) and the median, and whiskers show the maximum-minimum interval of two biological repeats with independent populations of plants. Individual biological repeats are represented with different shapes (n = 20 seedlings, 10 seedlings per biological repeat). Letters [a–c] denote groups that show statistically significant differences with other genotypes or treatments (within the same filament nucleation subclass) by two-way ANOVA with Tukey's post-hoc test ($P < 0.05$). **B)** Analysis of the population distribution of actin filament elongation rates. The elongation rate distribution of DMSO-treated wild type had a single peak at 1.25 – 1.75 µm/s, the DMSO-treated *arp2-1* had three peaks at 0.75 – 1.0 µm/s, 2.0 – 2.5 µm/s and > 3 µm/s, the SMIFH2-treated wild-type had a peak at 1.0 – 1.75 µm/s, but SMIFH2-treated *arp2-1* had peaks at 1.0 – 1.25 µm/s and 1.75 – 2.0 µm/s. n ≥ 100 single filaments from two individual biological repeats (for one biological repeat, 5 single filaments were counted in one hypocotyl from at least 10 hypocotyls per genotype or treatment). Letters [a–d] denote genotypes or treatments that show statistically significant differences with other groups by Chi-squared test, $P < 0.05$. **F–H)**, The average maximum length of filaments that originated *de novo* or from side-branching events in SMIFH2-treated *arp2-1* was significantly shorter than that in other cells, but filaments that originated from pre-existing ends did not show a difference between any genotype or treatment. **I–K)**, The average maximum lifetime of side-branching filaments in DMSO-treated *arp2-1*, SMIFH2-treated *arp2-1* and SMIFH2-treated wild-type cells were all significantly longer than the ones from DMSO-treated wild-type cells; however, filaments that originated *de novo* did not show any significant difference, and filaments that elongated from pre-existing ends in DMSO-treated wild-type cells were slightly shorter than SMIFH2-treated cells. **L–N)**, The severing frequency did not show any significant difference between different genotypes or treatments. In box-and-whisker plots, boxes show the interquartile range (IQR) and the median, and whiskers show the maximum-minimum interval of two biological repeats with independent populations of plants. Individual biological repeats are represented with different shapes (n = 20 seedlings, 10 seedlings per biological repeat). Letters [a–c] denote groups that show statistically significant differences with other genotypes or treatments (within the same filament nucleation subclass) by two-way ANOVA with Tukey's post-hoc test ($P < 0.05$).

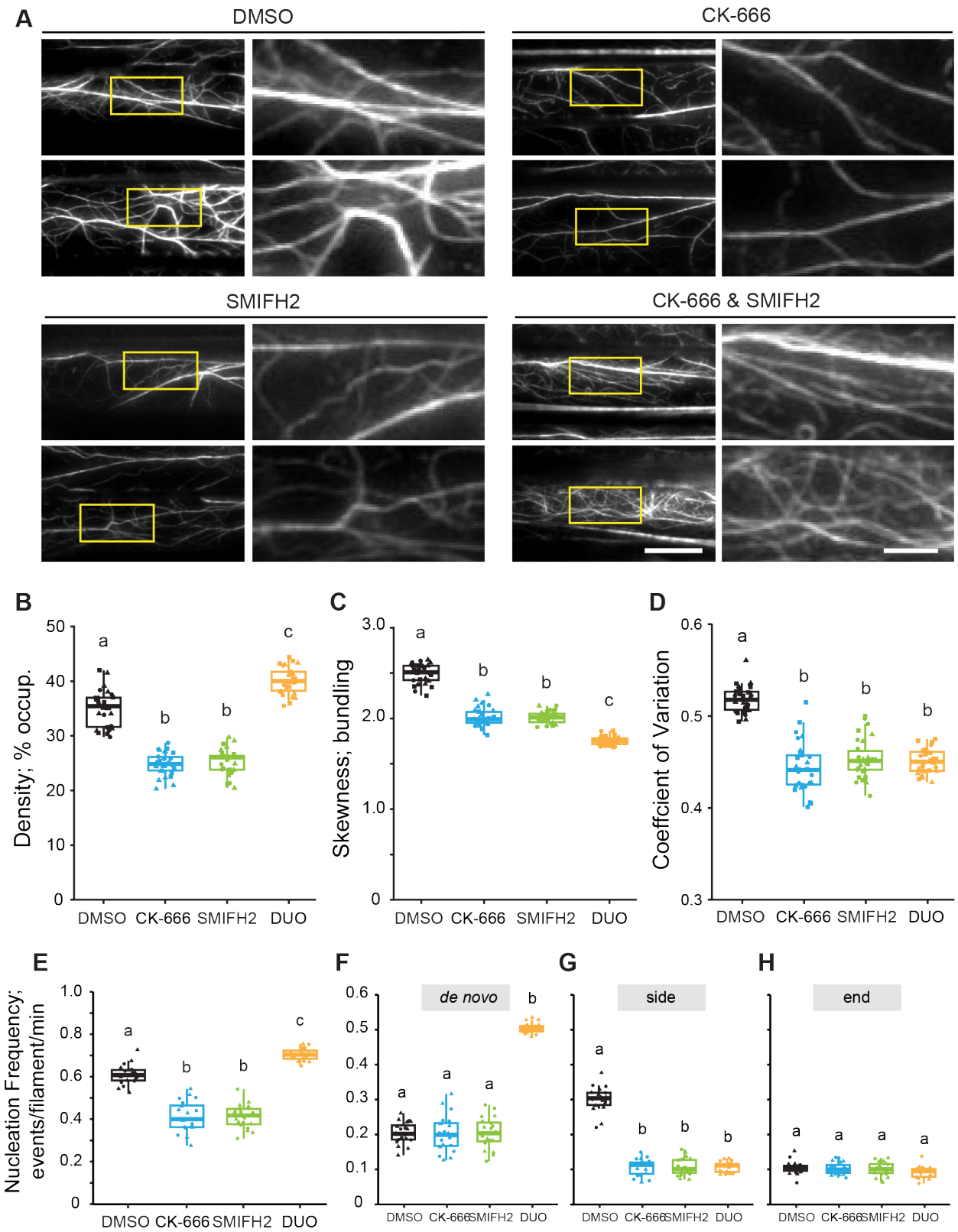
A
DMSO
CK-666
SMIFH2
CK-666 & SMIFH2
B
Density; % occup.
C
Skewness; bundling
D
Coeffcient of Variation
E
Nucleation Frequency; events/filament/min
F
de novo
G
side
H
end
DMSO
CK-666
SMIFH2
DUO

Figure 7. Filament abundance, total nucleation events and *de novo* filament formation increase when the Arp2/3 complex and formin activity are simultaneously reduced with chemical inhibitors.

A) Representative images of epidermal cells from the apical region of 5-d-old etiolated hypocotyls are shown in left columns. Scale bar: 20 µm. Regions of interest (yellow boxes) were magnified and displayed in right columns. Scale bar: 5 µm. Hypocotyls were treated with 0.05% DMSO solution, 10 µM CK-666, 25 µM SMIFH2 or both inhibitors for 5 min prior to imaging with VAEM. Actin filament arrays in CK-666-treated cells and SMIFH2-treated cells appeared to be less dense and less bundled compared to mock-treated cells. However, dual treatment markedly increased actin filament abundance. **B–D)** Quantitative analysis of actin filament density **(B)** and extent of bundling by skewness **(C)** and coefficient of variation **(D)** analyses. The density of actin arrays in CK-666-treated and SMIFH2-treated cells was decreased compared to mock-treated cells; however, dual-treated (DUO) cells had significantly increased actin density compared to all other treatments. Actin arrays in CK-666- or dual-treated cells were significantly less bundled than in mock-treated cells. In box-and-whisker plots, boxes show the interquartile range (IQR) and the median, and whiskers show the maximum-minimum interval of three biological repeats with independent populations of plants. Individual biological repeats are represented with different shapes (n = 30 seedlings, 10 seedlings per biological repeat). Letters [a–c] denote groups that show statistically significant differences with other genotypes or treatments by two-way ANOVA with Tukey's post-hoc test ($P < 0.05$). **E–H)** Quantitative analysis of actin filament nucleation frequency, both overall **(E)** and by subclass of origin **(F– H)**. The total nucleation frequency in mock-treated cells was higher than CK-666-treated and SMIFH2-treated cells. However, the total nucleation frequency of dual-treated (DUO) cells was significantly higher than all other treatments and this correlated with increased *de novo* nucleation events. In box-and-whisker plots, boxes show the interquartile range (IQR) and the median, and whiskers show the maximum-minimum interval of two biological repeats with independent populations of plants. Individual biological repeats are represented with different shapes (n = 20 seedlings, 10 seedlings per biological repeat). Letters [a–c] denote groups that show statistically significant differences with other genotypes or treatments by two-way ANOVA with Tukey's post-hoc test ($P < 0.05$).

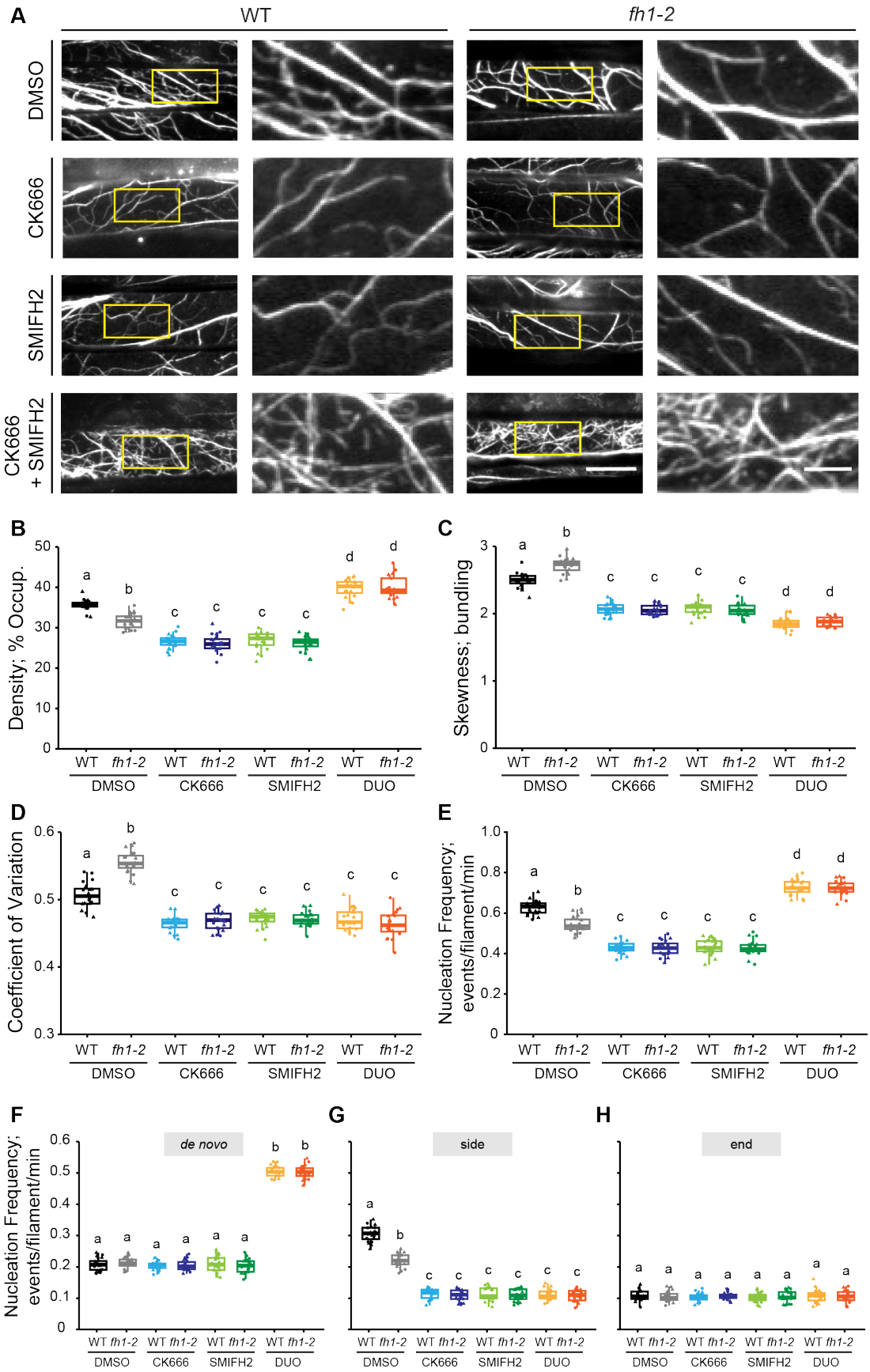
A
WT
fh1-2
DMSO
CK666
SMIFH2
CK666 + SMIFH2
B
Density; % Occup.
C
Skewness; bundling
D
Coefficient of Variation
E
Nucleation Frequency; events/filament/min
F
de novo
G
side
H
end
WT
fh1-2
DMSO
CK666
SMIFH2
DUO

Figure 8. SMIFH2 treatment results in further reduction of both actin density and actin filament nucleation frequency in the *fh1-2* mutant.

A) Representative images of epidermal cells from the apical region of 5-d-old etiolated hypocotyls are shown in the left columns. Scale bar: 20 µm. Regions of interest (yellow boxes) were magnified and displayed in the right columns. Scale bar: 5 µm. Hypocotyls were treated with 0.05% DMSO solution, 10 µM CK-666, 25 µM SMIFH2 or both inhibitors for 5 min prior to imaging. Actin filament arrays in either DMSO-treated or single-inhibitor-treated *fh1-2* cells all appeared to be less dense compared to DMSO-treated wild-type cells, but both dual-inhibitor-treated wild-type and *fh1-2* cells appeared to have more dense actin arrays compared to DMSO-treated wild-type cells. **B–D)** Quantitative analysis of the percentage of occupancy or density of actin filament arrays **(B)** and the extent of filament bundling as measured by skewness **(C)** and coefficient of variance **(D)** analyses. The density of actin arrays in DMSO-treated *fh1-2* cells was significantly decreased but the extent of filament bundling was increased compared to DMSO-treated wild-type cells. Treatment with either CK-666 or SMIFH2 caused an additional decrease in actin density in *fh1-2* cells and filaments were less bundled compared to DMSO-treated wild-type. However, simultaneous treatment with both inhibitors (DUO) significantly increased actin array density in both wild-type and *fh1-2* cells. In box-and-whisker plots, boxes show the interquartile range (IQR) and the median, and whiskers show the maximum-minimum interval of two biological repeats with independent populations of plants. Individual biological repeats are represented with different shapes (n = 20 seedlings, 10 seedlings per biological repeat). Letters [a–d] denote groups that show statistically significant differences with other genotypes or treatments by two-way ANOVA with Tukey's post-hoc test ($P < 0.05$). **E–H)** Quantitative analysis of actin filament nucleation frequency, both overall **(E)** and by subclass of origin **(F–H)**. The total nucleation frequency in DMSO-treated *fh1-2* cells was significantly reduced compared to DMSO-treated wild-type cells, and either CK-666 or SMIFH2 treatment caused an additional decrease in overall filament nucleation in *fh1-2* cells **(E)**. However, the total nucleation frequency of dual-inhibitor-treated *fh1-2* or wild-type cells was significantly higher than all other genotypes and treatments **(E)** and this correlated with increased *de novo* nucleation events **(F)**. In box-and-whisker plots, boxes show the interquartile range (IQR) and the median, and whiskers show the maximum-minimum interval of two biological repeats with independent populations of plants. Individual biological repeats are represented with different shapes (n = 20 seedlings, 10 seedlings per biological repeat). Letters [a–d] denote groups that show statistically significant differences with other genotypes or treatments by two-way ANOVA with Tukey's post-hoc test ($P < 0.05$).

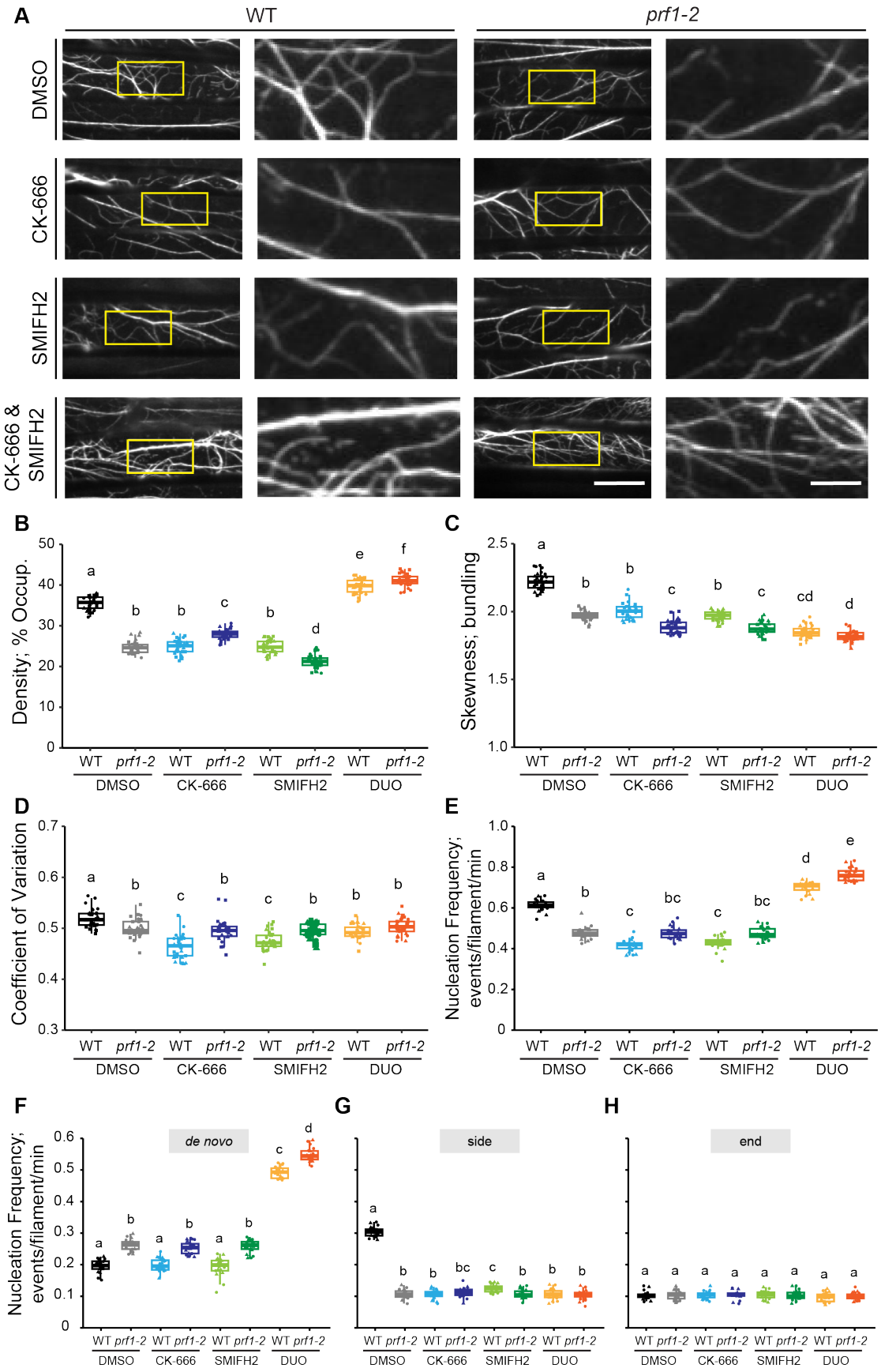
A
WT
prf1-2
DMSO
CK-666
SMIFH2
CK-666 & SMIFH2
B
Density; % Occup.
C
Skewness; bundling
D
Coefficient of Variation
E
Nucleation Frequency; events/filament/min
F
de novo
G
side
H
end
WT prf1-2 WT prf1-2 WT prf1-2 WT prf1-2
DMSO CK-666 SMIFH2 DUO

Figure 9. Increased filament abundance, total nucleation events and *de novo* filament formation following simultaneous CK-666 and SMIFH2 treatment are further enhanced in the *prf1-2* mutant.

A) Representative images of epidermal cells from the apical region of 5-d-old etiolated hypocotyls are shown in the left columns. Scale bar: 20 µm. Regions of interest (yellow boxes) were magnified and displayed in the right columns. Scale bar: 5 µm. Hypocotyls were treated with 0.05% DMSO solution, 10 µM CK-666, 25 µM SMIFH2 or both inhibitors for 5 min prior to imaging with VAEM. Actin filament arrays in either DMSO-treated or single-inhibitor-treated *prf1-2* cells all appeared to be less dense and less bundled compared to DMSO-treated wild-type cells, but both dual-inhibitor-treated wild-type and *prf1-2* cells appeared to have more dense actin arrays compared to DMSO-treated wild-type cells. **B–D)** Quantitative analysis of actin filament density **(B)** and extent of bundling by skewness **(C)** and coefficient of variation **(D)** analyses. The density of actin arrays in either DMSO-treated or single-inhibitor-treated *prf1-2* cells was significantly decreased compared to DMSO-treated wild-type cells; however, the treatment with both inhibitors (DUO) significantly increased the actin density in both wild-type and *prf1-2* cells. Actin arrays were less bundled when either Arp2/3, formins or PRF1 were inhibited compared to DMSO-wild-type cells. In box-and-whisker plots, boxes show the interquartile range (IQR) and the median, and whiskers show the maximum-minimum interval of three biological repeats with independent populations of plants. Individual biological repeats are represented with different shapes (n = 30 seedlings, 10 seedlings per biological repeat). Letters [a–f] denote groups that show statistically significant differences with other genotypes or treatments by two-way ANOVA with Tukey's post-hoc test ($P < 0.05$). **E–H)** Quantitative analysis of actin filament nucleation frequency, both overall **(E)** and by subclass of origin **(F–H)**. The total nucleation frequency in DMSO-treated, CK-666-treated and SMIFH2-treated *prf1-2* cells was significantly reduced compared to DMSO-treated wild-type cells. However, the total nucleation frequency of dual-inhibitor-treated (DUO) *prf1-2* **(E)** was significantly higher than all other genotypes and treatments and this corresponded to a significant increase in *de novo* nucleation events **(F)**. In box-and-whisker plots, boxes show the interquartile range (IQR) and the median, and whiskers show the maximum-minimum interval of two biological repeats with independent populations of plants. Individual biological repeats are represented with different shapes (n = 20 seedlings, 10 seedlings per biological repeat). Letters [a–e] denote groups that show statistically significant differences with other genotypes or treatments by two-way ANOVA with Tukey's post-hoc test ($P < 0.05$).